

Transfer efficiency enhancement and eigenstate properties in locally symmetric disordered finite chains

C. V. Morfonios^a, M. Röntgen^a, F. K. Diakonov^b, P. Schmelcher^{a,c}

^aZentrum für Optische Quantentechnologien, Universität Hamburg, Luruper Chaussee 149, 22761 Hamburg, Germany

^bDepartment of Physics, University of Athens, Panepistimiopolis, 15771 Athens, Greece

^cThe Hamburg Centre for Ultrafast Imaging, Universität Hamburg, 22761 Hamburg, Germany

Journal reference: *Annals of Physics* **418**, 168163 (2020)

Abstract

The impact of local reflection symmetry on wave localization and transport within finite disordered chains is investigated. Local symmetries thereby play the role of a spatial correlation of variable range in the finite system. We find that, on ensemble average, the chain eigenstates become more fragmented spatially for intermediate average symmetry domain sizes, depending on the degree of disorder. This is caused by the partial formation of states with approximate local parity confined within fictitious, disorder-induced double wells and perturbed by the coupling to adjacent domains. The dynamical evolution of wave-packets shows that the average site-resolved transfer efficiency is enhanced between regions connected by local symmetry. The transfer may further be drastically amplified in the presence of spatial overlap between the symmetry domains, and in particular when global and local symmetry coexist. Applicable to generic discrete models for matter and light waves, our work provides a perspective to understand and exploit the impact of local order at multiple scales in complex systems.

Keywords: Local reflection symmetry, Disorder, Transfer efficiency, Discrete Schrödinger equation

1. Introduction

Since the pioneering theoretical work by Anderson [1] it has been shown that, under many circumstances, spatial disorder in a medium leads to the exponential localization of waves due to multiple destructive interference. This behavior in turn suppresses the transport of an initial wave excitation through a disordered sample between remote sites. Initially explored for electrons in models of solids [1, 2], disorder-induced localization has more recently also been demonstrated and intensively studied for light waves [3, 4, 5, 6] as well as for matter waves in optical lattices [7, 8, 9]. Typically manifest in one-dimensional (1d) discrete lattice models with random onsite potential (diagonal disorder) or inter-site hoppings (off-diagonal disorder) [10, 11], localization also occurs for structural disorder in systems with binary constituents [5, 12] and may further be induced in the bulk of setups with disordered boundary [13].

The presence of spatial correlations between the constituents of an otherwise disordered medium generally causes wave excitations to be less localized and enhances transport, with the detailed system response depending on the type of correlated disorder [14]. Correlation can be short-ranged [15, 16], in the form of ordered clustered elements such as dimers [12, 17, 18, 19], trimers [20], or polymers [21, 22], it can have long-range character [14, 23, 24], while also mixed short- and long-range correlations [25] as well as subsystem disorder [26] have been explored. Further, delocalization may be facilitated by correlations between onsite elements alone [27], between hoppings [24], or between onsite and hopping elements [17].

In the meanwhile vast literature on wave localization, the impact of *spatial symmetry* has largely been used on the small scale of lattice constituents in resonant conditions of transport. On the other hand, a series of recent studies shows that the presence of global *centrosymmetry* [28]—equivalent to reflection symmetry for 1d systems—in an otherwise disordered finite system may lead to a prevalence of extended states and thereby enhance wave transfer between symmetry related sites [28, 29, 30, 31]. This principle applies to general multi-dimensional networks of interconnected nodes, even in the presence of many-body interactions [32, 33]. The effect is closely connected to the definite parity of the system eigenmodes which may result in correspondingly more extended states on configuration average [30]. Exploiting this property, global reflection

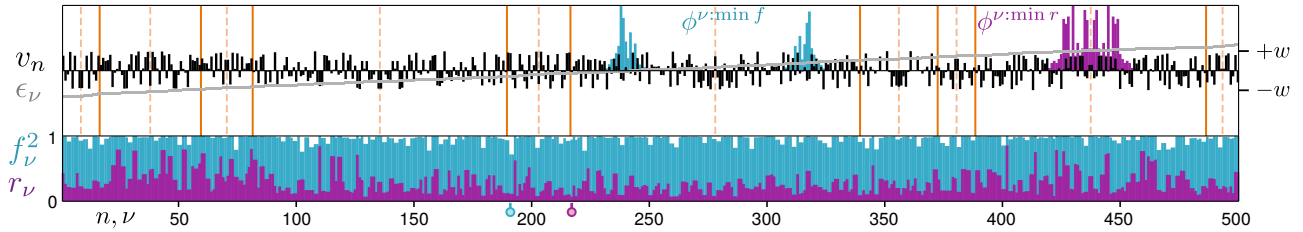


Figure 1: **Top:** Locally reflection-symmetric disordered (LRD) chain of $N = 500$ sites for disorder strength $w = 3h$, with initially random onsite elements $v_n \in [-w, w]$ symmetrized around local symmetry centers $c_{d=1,2,\dots,D}$ (vertical dashed lines) of $D = 10$ domains attached at random interfaces (vertical solid lines), and corresponding Hamiltonian eigenvalues ϵ_ν , for uniform hopping h (set to 0.01). **Bottom:** Inverse participation ratio (IPR) r_ν and cumulative Friedel sum (CFS) f_ν for increasing eigenstate index $\nu \in [1, N]$. The purple (blue) circle indicates the eigenmode of minimal r_ν (f_ν), with correspondingly colored modulus $|\phi_n^\nu|$ plotted in the top panel.

symmetry has also been proposed as a generator of tunneling in 1d disordered potentials with applications to secure communication in classical circuits [34]. The behavior of such globally symmetric systems in terms of optimal transfer efficiency is subject to further design conditions [28, 29], but generally demonstrates the crucial role of symmetry coexisting with disorder.

In fact, global symmetry is seldom exactly fulfilled. Continuous symmetry measures [35] and symmetry operation measures [36] have been proposed to describe deviation from exact symmetry. A different paradigm of global symmetry breaking is the case of exact but *local* symmetries, that is, symmetries which are fulfilled in a restricted subdomain of a composite system. A recently developed theoretical framework addresses such local symmetries in terms of symmetry-adapted non-local currents [37] governed by generalized non-local continuity equations [38, 39]. Their stationary versions reveal the presence of 1d local symmetries in generic wave-mechanical systems including non-Hermitian [38, 40] or even driven [38, 41] setups. In particular, they enable amplitude mappings which generalize the parity and Bloch theorems to the case of local symmetry [42], and can be used to classify perfectly transmitting states [38, 43]. A well-known class of systems featuring abundant local symmetries is that of 1d binary deterministic aperiodic structures (see e. g. Ref. [44] and references therein), where their combinatorial properties have been studied in terms of the so-called “palindrome complexity” [45]. Local symmetries may generally also be found “hidden” [46] in amorphous and disordered systems [47] where their presence may affect order-disorder transitions [48], or exist “concurrently” in interplay with global symmetries within molecules [49]. Ultimately, any system with global symmetry which is coupled to an environment can be considered locally symmetric. In view of the manifest role of global symmetry, this abundance of local symmetries raises the question of their impact on localization and transfer when multiply present at different locations and scales in disordered systems.

We here view local reflection symmetry, defined within different spatial subparts of a system, as a particular type of correlation of fixed or variable range in an otherwise disordered finite system. To study the effect solely of local symmetry in a simple setting, we consider finite 1d tight-binding chains with disordered onsite potentials which are mirror-symmetrized within adjacent or overlapping spatial domains of random or uniform size. The localization properties of the eigenstates of such locally reflection-symmetric disordered (LRD) chains are then studied numerically for varying disorder strength and symmetry domain sizes (for brevity, from now on “symmetry” will refer exclusively to reflection symmetry, unless otherwise stated). Apart from the widely used inverse participation ratio [50], we utilize a recently proposed [51] alternative localization measure which reflects the fragmentation of states induced by the local symmetries. An intricate interplay between the short-range localization and long-range fragmentation properties is observed. It indicates an overall change to more fragmented states, within the ensemble average, for intermediate degree of local symmetry, with the uncorrelated case recovered in the limit of small symmetry domains. This behavior is analyzed by combining the notion of fictitious disorder-induced tunneling barriers with the concept of symmetrization of eigenstates into symmetry domains, in turn explained within a local resonant scattering picture. A crucial ingredient is here the concept of approximate *local parity* [37, 38, 42] of localized eigenstates within symmetry domains perturbed by the coupling to adjacent domains. Notably, the purpose here is to investigate the effect of the local symmetry correlations on the properties of *finite* LRD chains, which do not serve to approximate the large chain

limit; they are simply chosen large enough to vary the number of symmetry domains and to perform eigenstate statistics. Ultimately, we explore the impact of local symmetry on the diffusion of time-evolved wave-packets, by computing statistical distributions of the site-resolved transfer efficiency upon a single site excitation in LRD chains with few symmetry domains. We here show that local symmetry may significantly enhance the transfer depending on the domain configurations. A drastic increase in transfer is shown to occur when symmetry domains overlap with each other. In particular, the transfer enhancement induced by global symmetry can be further increased considerably when local symmetry is present simultaneously at smaller scales.

The paper is organized as follows. In Sec. 2 we first define the considered LRD chain setups and provide the analysis tools used to distinguish localization from fragmentation (Sec. 2.1). We then classify the types of eigenstate profiles present in the LRD chains (Sec. 2.2) which are employed to explain the distribution of the computed localization measures for varying disorder and symmetry (Sec. 2.3). In Sec. 3 we investigate wave-packet dynamics in LRD chains, demonstrating the enhancement of transfer efficiency via local symmetry (Sec. 3.1) and its further increase in the presence of symmetry domain overlaps (Sec. 3.2). Section 4 concludes our investigations. Appendix A explains the typical ‘‘symmetrization’’ of eigenstates into symmetry domains and Appendix B provides a mapping of such eigenstates to ‘‘fictitious’’ double wells. Appendix C corroborates the localization features with eigenstate symmetrization statistics, Appendix D analyzes the effect of global symmetry and its statistics for larger chains, and Appendix E focuses on the spectral statistics of LRD chains.

2. Eigenstate fragmentation in locally reflection-symmetric disordered (LRD) lattices

We consider a generic 1d chain of N sites with uniform real next-neighbor hopping h described by the single-particle Hamiltonian

$$H = \sum_n v_n |n\rangle \langle n| + \sum_{|m-n|=1} h |m\rangle \langle n| \quad (1)$$

where v_n is the onsite potential of site n with single site orbital $|n\rangle$. The onsite potential values are taken from a uniform random distribution with magnitude up to a disorder strength parameter w , that is, $v_n \in [-w, +w]$. The potential array is then locally symmetrized within D adjacent domains \mathbb{D}_d ($d = 1, 2, \dots, D$) of sizes (that is, number of contained sites) N_d , starting from the left. The resulting chain is thus symmetric under the action of D local reflection transformations $\mathcal{P}_{c_d; N_d} \equiv \mathcal{P}_{\mathbb{D}_d}$, each of which performs a permutation of sites only within domain \mathbb{D}_d about its center c_d and acts as the identity on the rest of the chain [37, 38],

$$\mathcal{P}_{\mathbb{D}_d} : n \rightarrow \begin{cases} 2c_d - n, & n \in \mathbb{D}_d \\ n, & n \notin \mathbb{D}_d \end{cases} \quad (2)$$

In other words, our chain can be constructed by concatenating D reflection symmetric subdomains. In order to study the impact solely of the presence of local symmetry, to begin with the N_d are also taken at random from a uniform distribution, obeying $\sum_d N_d = N$ with $N_d \geq 1$. A correlation of spatially variable range N_d is therefore induced into the otherwise disordered chain. Such a configuration is shown in Fig. 1 (top panel).

In the following we investigate the localization properties of the eigenvectors $|\phi^\nu\rangle = \sum_n \phi_n^\nu |n\rangle$ of H , given by

$$H |\phi^\nu\rangle = \epsilon_\nu |\phi^\nu\rangle, \quad (3)$$

with eigenvalues ϵ_ν . The spatial profiles of the squared eigenmode norms $\rho_n^\nu = |\phi_n^\nu|^2$ are unaffected by the sign of the hopping h which induces a relative $\pi/2$ phase flip between adjacent sites [52]. We have here chosen $h > 0$, modeling e. g. the evanescent coupling between photonic waveguides, while the choice $h < 0$ would correspond to e. g. the kinetic energy of non-interacting electrons on a tight-binding lattice.

2.1. Localization versus fragmentation of states

A convenient and widely used single-parameter indicator of the grade of localization of a wavefunction is the inverse participation ratio (IPR) defined by [50]

$$r = \sum_{n=1}^N \rho_n^2 \in [N^{-1}, 1] \quad (4)$$

for a normalized state $|\psi\rangle$ of squared modulus $\rho_n = |\psi_n|^2$ (with $\sum_{n=1}^N \rho_n = 1$). The IPR takes on its maximal value $r = 1$ in the limit of a state localized on a single site m , $\rho_n = \delta_{mn}$, and its minimal value $r = 1/N$ for a state uniformly extended over the chain, $\rho_n = 1/N$. As desired for a localization measure, the IPR does not depend on the position at which a state is localized within a disordered system. At the same time, however, it is also largely insensitive to the spatial state profiles [51], which in general do affect the static properties and dynamical response of the system. An alternative localization measure, proposed very recently in Ref. [51] and inspired by the Friedel sum rule [53], reflects more details of the spatial profile ρ_m by using its cumulative sum $P_n = \sum_{m=1}^n \rho_m$ up to site n . We slightly redefine (see comment below) the measure here as

$$f = \frac{1}{2N} \left| \sum_{n=1}^N (e^{2\pi i P_n} + 1) \right| \in [N^{-1}, 1], \quad (5)$$

which we will refer to as the ‘‘cumulative Friedel sum’’ (CFS) of a given state. Again, larger (smaller) CFS indicates a more (less) localized state, though now taking into account its total spatial extent instead of only its site participation, as described in the following.

The IPR and CFS distributions among the eigenmodes of a single LRD chain configuration are shown in the bottom panel of Fig. 1. An impression of the difference between IPR and CFS in indicating localization properties is provided by the eigenstates $\phi^{\nu:\min r}$ and $\phi^{\nu:\min f}$ in Fig. 1 having minimal r and f , respectively, for the example setup. With a similar density contribution (comparable amplitudes at similar number of sites), the states have almost the same IPR, which thus does not distinguish them. In contrast, the drastically smaller CFS of $\phi^{\nu:\min f}$ indicates its extended profile: The envelope consists of two individual maxima which are more peaked than in $\phi^{\nu:\min r}$, but lie farther apart, thus yielding an increased total extent. For (normalized) states with local maxima, the CFS can thus be seen to indicate the degree of spatial ‘‘fragmentation’’, that is, how remote from each other the amplitude maxima are located. As an example, if we consider a (virtual) normalized state consisting of two single-site peaks at spacing s and zero elsewhere in an N -site chain, then the CFS decreases monotonously from $f = 1$ at $s = 0$ (one single-site peak) to $f = 1/N$ at $s = N - 1$ (one peak at each end of the chain)¹. If each of the two peaks has a symmetric profile of common finite width (in the form of, e. g., a Gaussian or a rectangular step), then f is independent of this width. Thus, the CFS *complements* the IPR, as a localization measure which is sensitive to the spacing of peaks in a wavefunction but relatively insensitive to the width of the peaks themselves (except for single peaks, that is, of non-fragmented states).

Before we present the statistical behavior of the IPR and CFS in Sec. 2.3, we next provide an intuitive interpretational tool where the symmetry domains effectively behave like double wells perturbed by the coupling to adjacent domains.

2.2. Eigenstate symmetrization

The qualitative distinction between the IPR and CFS in the present context of LRD chains is closely linked to the fact that, as explained in Appendix A, the eigenstates generally tend to ‘‘symmetrize’’ into the symmetric chain domains. By this we mean that, for a sufficiently localized eigenvector $|\phi^\nu\rangle$ in a LRD finite chain, the density will have the *approximate symmetry* $\rho_n \approx \rho_{2c_d-n}$ about the center c_d of some domain $\mathbb{D}_d \ni n$, while approximately *vanishing outside* of it, $\rho_{n \notin \mathbb{D}_d} \approx 0$. Examples of this are states $\phi^{\nu:\min r}$ and $\phi^{\nu:\min f}$ already seen in Fig. 1. In other words, the states tend to become approximate *local parity eigenstates* [38] of local reflections $\mathcal{P}_{\mathbb{D}_d}$ as defined in Eq.(2)².

Further, as explained in Appendix B, each such locally symmetrized eigenstate can be mapped to a ‘‘*fictitious double well*’’ with constant inter-well barrier strength $\tilde{v} = \tilde{v}^\nu$ and of width $\xi = \xi_d^\nu$ (corresponding to state $|\phi^\nu\rangle$ symmetrized into domain \mathbb{D}_d) given by the spacing between the state’s maxima; see Eqs.(B.1) and (B.2), respectively. This mapping is visualized in Fig. 2 (a) for a selected state localized in domain \mathbb{D}_7 of the setup in

¹For comparison, the measure $|\sum_{n=1}^N e^{2\pi i P_n}/N|$ in Ref. [51] would tend to 0 for spacing $s \rightarrow N/2$ for large N and then rise towards 1 again for $s \rightarrow N$. This would make its value ambiguous for (locally) symmetric ρ_n with large spacings. We have therefore redefined the measure into f in Eq.(5) to better serve the present study.

²Note that local symmetry in ρ_n is not automatically fulfilled by a symmetry in the total Hamiltonian. Indeed, despite the geometric symmetry of the chain under the $\mathcal{P}_{\mathbb{D}_d}$, those operations do not commute with H since they do not preserve the connectivity of the chain [38]: Domain end sites are coupled to different sites upon transformation.

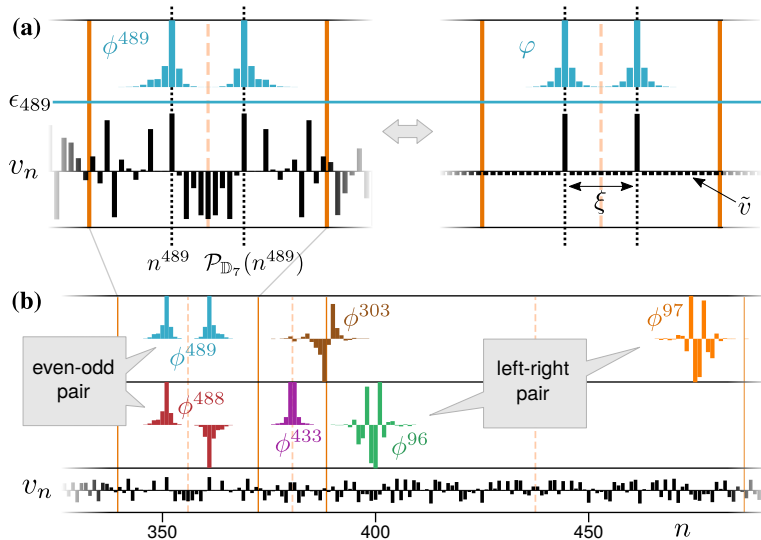


Figure 2: **(a)** Focus on (*left*) the eigenstate ϕ^{489} localized symmetrically in domain \mathbb{D}_7 of the chain in Fig. 1, with potential v_n shown in arbitrary units, and (*right*) the corresponding “fictitious” state φ decaying exponentially away from the maximum positions $n_\nu, \mathcal{P}_{\mathbb{D}_d}(n_\nu)$ within a constant potential \tilde{v} (see Eq. (B.1)), with the potential at $n_\nu, \mathcal{P}_{\mathbb{D}_d}(n_\nu)$ tuned so that φ ’s energy equals ϵ_{489} (indicated by dotted line). The disordered symmetry domain is thus associated to a fictitious double well with barrier width ξ (see Eq. (B.2)) for this particular (symmetrized) eigenstate. **(b)** State types in the LRD chain of Fig. 1: Even-odd state pair (with indices $\nu = 488, 489$) in domain \mathbb{D}_7 , left-right state pair ($\nu = 96, 97$) in \mathbb{D}_9 , single even state ($\nu = 433$) in \mathbb{D}_8 , and asymmetric state ($\nu = 303$) localized at the boundary between \mathbb{D}_8 and \mathbb{D}_9 . States are normalized to maximum modulus and plotted offset for visibility.

Fig. 1. Notably, for the eigenstate symmetrization to occur in a domain \mathbb{D}_d , the short-range localization length ℓ of the state (see Appendix B) should be significantly smaller than that domain’s size N_d .

In terms of local symmetry, the eigenstates of a finite LRD chain will in general be of one of the following types, with examples shown in Fig. 2 (b):

(i) “Even-odd” (*eo*) pair: two quasidegenerate states of approximate even and odd local parity, resembling the energy-split states of an isolated symmetric double well, with approximately the same density profile (see ϕ^{488}, ϕ^{489});

(ii) “Left-right” (*lr*) pair: two quasidegenerate states localized in the left and right half of a symmetry domain each, resembling the states of an isolated well and its mirror image, each with spatial state profile being approximately the mirror image—under $\mathcal{P}_{\mathbb{D}_d}$ —of the other (see ϕ^{96}, ϕ^{97});

(iii) Single states of approximate local (even or odd) parity (see ϕ^{433}), in cases where the above-mentioned fictitious barrier width ξ is of the order of the short-range localization length ℓ (see Appendix B);

(iv) Single asymmetric states localized around the boundary between two symmetry domains for sufficiently strong disorder (see ϕ^{303}) or extended over multiple domains for very weak disorder, sharing none of the above properties.

We emphasize here that the coupling of the symmetry domain boundaries to the surroundings (adjacent domains) acts as a *perturbation* on the local parity of domain-localized eigenstates. This perturbation increases with the overlap of those states with the domain boundaries, and depending on the fictitious inter-well barrier (see Appendix B), they may (like *eo* pairs) or may not (like *lr* pairs) have approximate local parity with respect to $\mathcal{P}_{\mathbb{D}_d}$. Indeed, *lr* pairs can be seen as originating from *eo* pair states which are practically degenerate due to vanishingly small inter-well coupling (large ξ_d^ν and/or \tilde{v}^ν of the fictitious barrier) and combine linearly into left- and right-localized states under the boundary perturbation³. In other words, a stronger disorder-induced fictitious double-well barrier assists the local parity breaking caused by the coupling of the domain to its environment.

The IPR and CFS distribution among the eigenstates of a given LRD chain will highly depend on the occurrence of *eo* and *lr* pairs. For *eo* pair states, a localization peak at some position, denoted n_ν , within a

³Variants of *lr* pair states may thereby further occur which are mainly localized on one domain half but have a small amplitude also on the other half, resulting from the combination of *eo* pair states with slightly asymmetric (again due to broken parity) densities.

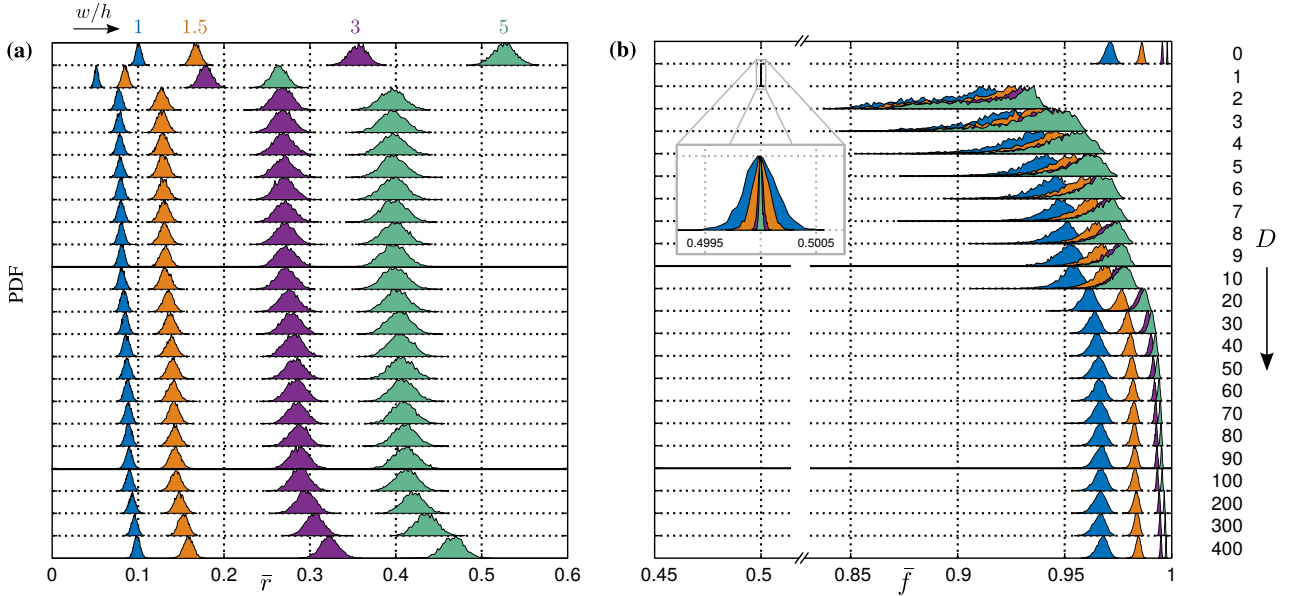


Figure 3: **(a)**: Probability density function (PDF) of mean inverse participation ratio (IPR) \bar{r} over the $N = 500$ eigenstates of a locally reflection-symmetric disordered (LRD) chain, for varying disorder strength w and number D of (randomly sized) symmetry domains, using 3000 random configurations. **(b)**: Same as in (a), but for the mean cumulative Friedel sum (CFS) \bar{f} . PDFs are normalized to maximum for each (w, D) pair.

symmetry domain \mathbb{D}_d imposes the same localization peak at $\mathcal{P}_{\mathbb{D}_d}(n_\nu)$. This yields relatively small IPR and CFS values, each with a double multiplicity (since the pair states have almost the same density)—as evident, e. g., from pairs of equal consecutive r_ν - or f_ν -bars in Fig. 1. The CFS will additionally decrease with the distance ξ_d^ν between the two density peaks which represents the degree of the state’s fragmentation mentioned in Sec. 2.1. In contrast, lr state pairs contribute with relatively high IPR and CFS values (now without fragmentation present), again with double multiplicity.

The relative frequency of eo and lr pairs will depend on the average fictitious double-well barriers emerging among the different domains. For a given moderate disorder strength, the key analysis tool is here the average of the fictitious barrier widths ξ_d^ν , which naturally follows the mean size of symmetry domains. Indeed, larger domain size N_d allows for larger ξ_d^ν corresponding to states which stochastically localize further from the domain center. This in turn favors the formation of lr pairs from boundary-perturbed combinations of eo pairs, as described above.

2.3. Statistical eigenstate spatial properties

With the above insight into individual eigenstate profile characteristics, we now analyze the statistical behavior of eigenstate localization in LRD chains for varying disorder and setup symmetrization. To this end, we compute [54] the probability distribution function (PDF) of the mean IPR \bar{r} and CFS \bar{f} over the eigenstates of a given configuration, where $\bar{x} = \sum_{\nu=1}^N x_\nu / N$ with $x = r, f$. The result is shown in Fig. 3 for different disorder strengths w and number of symmetry domains D . As we see, for each (w, D) -combination the IPR and CFS distributions have well-defined single maxima. Note that $D = 0$ represents a random chain without any symmetrization and $D = 1$ a globally symmetric disordered chain, while the maximal value $D = N$ (not shown) is equivalent to $D = 0$.

As expected, we see in Fig. 3(a) that the mean IPR is peaked at higher \bar{r} —that is, eigenstates are more localized—at stronger disorder, for any number of symmetry domains. Indeed, the Anderson localization mechanism will govern the spatial decay on the single-site length scale within the region where a state is concentrated, independently of the presence of symmetries on larger scales. Larger w then leads to faster decay and larger \bar{r} on average. At the same time, the fluctuations around the peak \bar{r} value (width of each PDF hump) increase with w , since individual r -values—being quadratic in ρ_n —are more sensitive to detailed differences between spatial configurations for more localized (larger ρ_n -values) states.

On top of those short-range statistical characteristics, Fig. 3(a) shows a systematic impact of the long-range spatial correlations of the chain on the IPR distributions induced by local symmetry (we comment explicitly

on the global symmetry case $D = 1$ later): For any disorder strength w , the PDFs shift to lower \bar{r} when adding local symmetry (from $D = 0$ to any $D \neq 0$), and rise to higher \bar{r} as D increases, approaching the random limit again at $D = N$. Let us analyze the PDF evolution with varying D more specifically as a result of the local symmetry-induced state profiles described in Sec. 2.2. Since increasing D yields smaller domains on average, it thereby also leads to smaller average widths ξ_d^ν of the fictitious double-well barriers (see Fig. 2(a)) induced by the disorder. This in turn favors the occurrence of eo state pairs (with relatively small IPR) compared to lr pairs (with relatively large IPR), as concluded in Sec. 2.2. At the same time, however, the occurrence of domain-interface-localized asymmetric states (of type (iv) in Sec. 2.2), of relatively large IPR, increases for larger number ($D - 1$) of domain interfaces. Also, eo pairs become less supported again for smaller domains where the states do not have enough available space to localize away from the parity-breaking domain boundaries. Together, these effects lead to a gradual increase of the mean IPRs for larger D towards the limit $D \rightarrow N$.

More striking aspects related to the spatial state profiles for different D and w are captured by the CFS distribution shown in Fig. 3(b). The short-range localization behavior of the mean CFS \bar{f} is similar to that of the IPR discussed above: For given D , the peak \bar{f} values increase with disorder strength w , indicating stronger localization. Interestingly, however, the fluctuations around the peaks show a behavior opposite to the IPRs at $D \gtrsim 10$, now being more enhanced for weaker disorder. This indicates that the average degree of spatial fragmentation (as measured by \bar{f}) is more homogeneous for large w with stronger short-range localization, while smaller w favors fragmentation variability for the more smeared out states. Also, the \bar{f} -fluctuations increase for smaller number of domains (towards $D = 2$), since there the range of variability in the domain sizes N_d increases.

The evolution of the CFSs with varying domain number D generally follows the same scheme as the IPRs, with an initial shift to smaller \bar{f} with the onset of local symmetry and a gradual recovering of the random limit as $D \rightarrow N$. Complementing the IPRs as an eigenstate fragmentation measure, the CFSs reveal the role of eo state pairs in a more resolved manner with increasing D . Specifically, smaller domains (smaller fictitious intra-domain barrier widths ξ_d^ν) on average favor the occurrence of eo over lr pairs, and thus the CFSs systematically increase with the decreasing fragmentation of eo states. At the same time, the fluctuations around the CFS peaks decrease with D since the smaller domains allow for smaller variation in the extent of symmetrized states.

For a more complete picture of the above features, statistical distributions of the number of locally approximate even/odd and left-/right-localized states (including eo - and lr -pairs) are given in Appendix C for varying w and D . They demonstrate a gradual diminishing of domain-localized states with increasing D , though at a slower rate for locally even/odd than for left-/right-localized states.

An extreme manifestation of symmetry-induced localization in the IPR and CFS distributions naturally occurs for global symmetry ($D = 1$), where all eigenstates are even or odd. With a fixed domain size $N_1 = N$, the majority of eigenstates generally consists of eo pairs, inducing a dramatic jump of the PDFs to lower \bar{r} and \bar{f} . In particular, \bar{f} is sharply peaked at $1/2$ for all disorder strengths, indicating an average eo -state density peak spacing ξ of $N/2$ (recall the behavior of f from Sec. 2.1), with fluctuations decreasing with w . This feature is analyzed in detail in Appendix D, where also the dependence on the chain length is investigated.

Finally, it should be noted that, whereas the local symmetries have substantial impact on the chain eigenstates for different D , the corresponding eigenenergy spectra share the overall trend of uncorrelated random chains. More specifically, for sufficiently strong disorder the eigenenergies ϵ_ν tend to increase linearly with ν , as seen in Fig. 1 on the scale of the plot. The difference from a non-symmetrized chain lies in the occurrence of multiple quasidegeneracies on smaller scale (discernible when stretching the ϵ -axis) corresponding to eo or lr state pairs, as described above. A more detailed analysis of the spectrum of this exemplary LRD chain (with $D = 10$ domains) is given in Appendix E, together with the ensemble average thereof.

3. Transfer efficiency in LRD chains with adjacent and overlapping symmetry

Having investigated and explained the static eigenstate properties of LRD chains, let us now explore the impact of local symmetry on the dynamics of evolving wave-packets. Since any wave-packet will evolve according to its projection coefficients on the chain's eigenstates, the question of interest here will be whether the occurrence of approximate local parity eigenstates may systematically affect the dynamics.

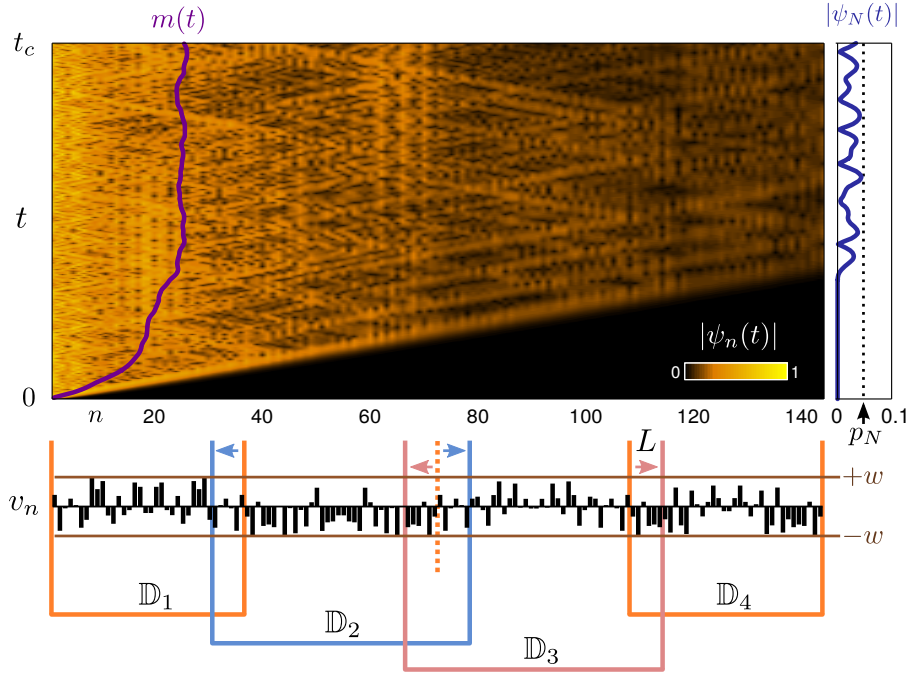


Figure 4: Wave-packet evolution $|\psi_n(t)|$ up to $t_c = 200/h$ with superimposed mean displacement $m(t)$ (top) upon unit excitation at site $n = 1$ of an LRD chain of disorder strength $w = h$ with $D = 4$ overlapping symmetry domains (bottom) where \mathbb{D}_2 and \mathbb{D}_3 have been extended symmetrically by L sites. The transfer efficiency p_N from first to last site is indicated (top right).

In the study of correlation-induced effects on wave diffusion during evolution, a widely used measure is the root-mean-square (standard) deviation, defined as [16]

$$m(t) = \sqrt{\sum_n (n - n_0)^2 |\psi_n(t)|^2} \quad (6)$$

for a discrete chain, where the wave-packet $|\psi(t)\rangle$ evolves here according to the Schrödinger equation (with $\hbar \equiv 1$)

$$i\partial_t |\psi(t)\rangle = H |\psi(t)\rangle \quad (7)$$

under an initial unit excitation at the single site n_0 , $|\psi(t=0)\rangle = |n_0\rangle$. Such an evolution is shown in Fig. 4 for initial excitation at the left end $n_0 = 1$ of an LRD chain. For simplicity, we have chosen a relatively short chain with a small number $D = 4$ of symmetry domains. In this example, however, we also introduce a spatial *overlap* between consecutive domains which, as we will see below, may drastically affect the diffusion. Specifically, in Fig. 4 the overlap is created by extending each domain except for the first (\mathbb{D}_1) and last (\mathbb{D}_D) by a fixed number of sites L , keeping the domain centers fixed.

The mean displacement $m(t)$ for the configuration in Fig. 4 increases with time, as expected, until $\psi_n(t)$ has spread enough to reach the right end where it is back-reflected.⁴ From this point on $m(t)$ simply fluctuates around a constant mean value. This is, nevertheless, the generic behavior also for uniformly random chains without local symmetry correlations, with the saturation mean value for $m(t)$ decreasing with disorder strength. For other types of (short- or long-range) correlation, the effect on the rate of increase of $m(t)$ is usually studied before reflection at the end of the chain sets in [17]. Local-symmetry-induced correlations, however, do not affect the overall displacement behavior on ensemble average: In analogy to the IPR used in Sec. 2, the mean displacement does not resolve details of the time-dependent spatial profile of $|\psi_n(t)|$ (like, e. g., the faint but visible slight enhancement of $|\psi_n(t)|$ close to the overlap between domains \mathbb{D}_2 and \mathbb{D}_3 seen in the color-plot of Fig. 4).

⁴Since we here explicitly investigate transfer in *finite* chains, we let the wave-packet reach the end of the chain, leading to a saturation of $m(t)$. This is in contrast to studies on approximants of infinite chains, where back-reflection of the wave is avoided and $m(t)$ increases as $\sim \sqrt{t}$ on average for uncorrelated disorder.

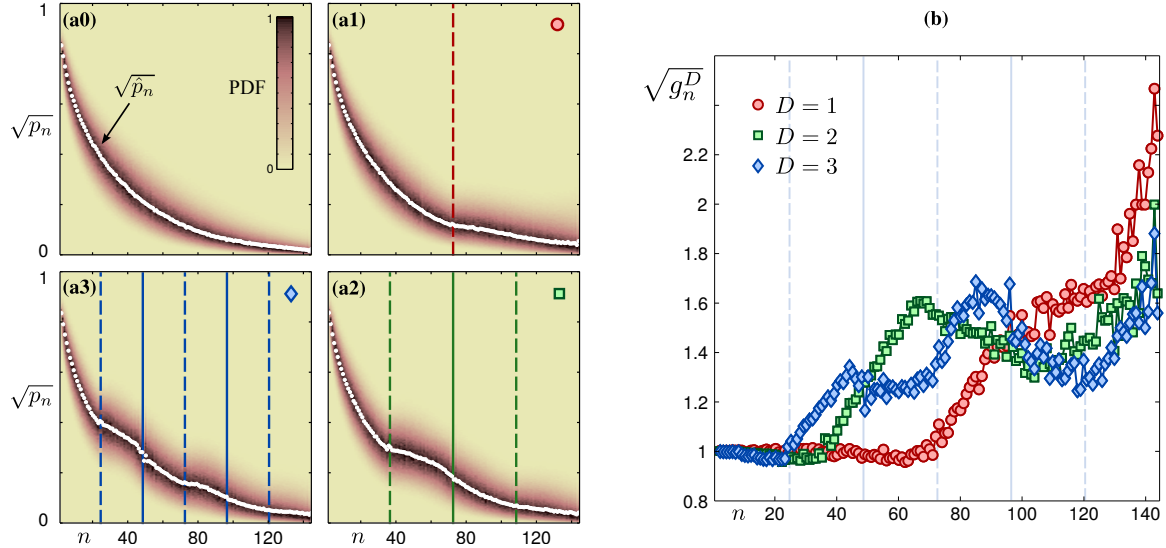


Figure 5: PDFs of scaled transfer efficiency p_n (normalized to maximum for each n) within cutoff time $t_c = 200/h$ (1000 time-steps), for an ensemble of 30 000 LRD chains ($N = 144$, $w = 1.2h$) with (a0) no symmetry ($D = 0$), (a1) global symmetry ($D = 1$), (a2) $D = 2$ and (a3) $D = 3$ adjacent symmetry domains, with PDF peak positions \hat{p}_n (white dots) estimated using local regression. Solid (dashed) vertical lines indicate domain interfaces (centers). (b) Transfer efficiency enhancement factor $g_n^D = \hat{p}_n^D / \hat{p}_n^0$ (scaled) for $D = 1, 2, 3$.

To probe possible symmetry-induced dynamical effects in the LRD chain in a site-resolved manner, we will utilize the so-called “transfer efficiency” [30, 28] of the initial excitation to site n , defined here as the maximum amplitude at n over a fixed reference time t_c ,

$$p_n = \max_{t \in [0, t_c]} |\langle n | e^{-iHt} | n_0 \rangle| = \max_{t \in [0, t_c]} |\psi_n(t)| \in [0, 1], \quad (8)$$

where we set the input site to $n_0 = 1$. To visualize an example, $p_{n=N}$ is indicated in Fig. 4 (right panel) for that setup. The transfer efficiency has been used to demonstrate that *global* symmetry in discrete disordered networks may generally lead to an enhanced signal transmission between diametrically located input and output end-sites [28]. This effect relies on the commutation of the Hamiltonian with the global reflection operation, and was shown to be subject to further conditions and optimizations when promoted for efficient quantum transport [30].

3.1. Transfer enhancement by local symmetry

What we aim to investigate here is whether a statistical enhancement of signal transfer (compared to uncorrelated disorder) can be manifest if more than one *local* symmetries are present in the finite chain, each of which now does not commute with H . To this end, we first consider the case of adjacent, that is, non-overlapping symmetry domains. We compute the PDFs of the site-resolved transfer efficiency p_n over an ensemble of disordered configurations of an $N = 144$ -site chain with $D = 1, 2, 3$ symmetry domains, and compare it to the non-symmetric, uniformly random case ($D = 0$). The results are shown in Fig. 5 (a0)–(a3), where $\sqrt{p_n}$ is plotted to increase detail visibility. We use here a disorder strength $w = 1.2h$ and evolution time $t_c = 200/h$ in Eq. (8) such that the wave-packet has explored the whole chain. As we see, in all cases the PDF for any given site n is rather peaked (with peaks becoming narrower towards the chain ends), and the peak p_n -values fall monotonously with n , as can be anticipated for a disordered chain. Notably, one can clearly distinguish a relatively small but statistically systematic enhancement of p_n when local symmetry is imposed, approximately in the right halves of the symmetry domains; see local humps of PDF peaks along n in Fig. 5 (a1),(a2),(a3).

For a clearer comparison with the non-symmetric case (a0), Fig. 5 (b) shows (scaled) the enhancement quotient

$$g_n^D = \frac{\hat{p}_n^D}{\hat{p}_n^0} \quad (9)$$

of the peak transfer efficiencies \hat{p}_n^D (corresponding to $D = 1, 2, 3$ domains) to that of the uncorrelated random chain, \hat{p}_n^0 . The PDF peak values (white dots in Fig. 5 (a0)–(a3)) have been estimated as the maxima of smoothed

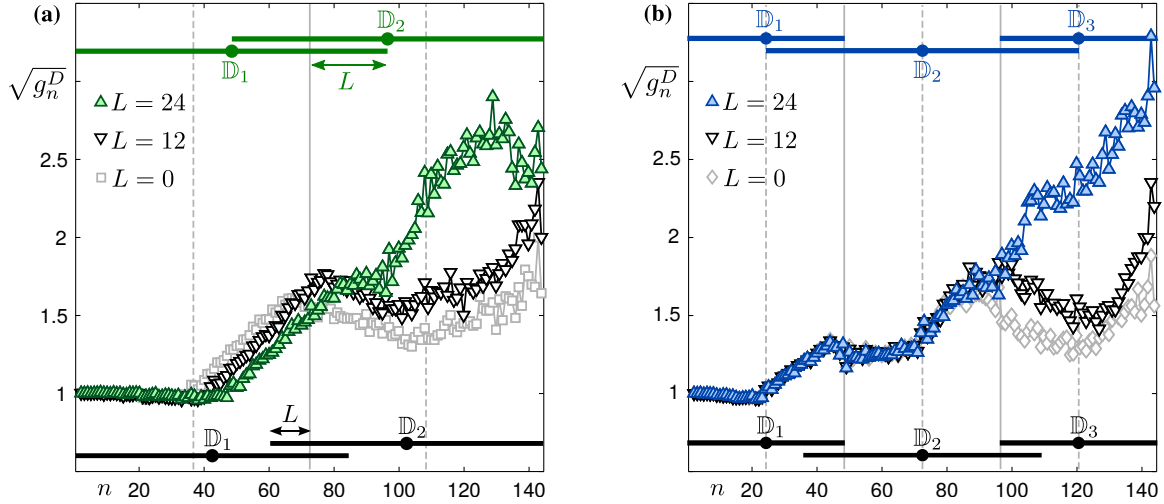


Figure 6: Transfer efficiency enhancement factor g_n^D (scaled) like in Fig. 5 (b) but for finite overlap between symmetry domains created by (a) extending each of $D = 2$ domains by L sites across the chain center and (b) extending the middle one of $D = 3$ domains symmetrically by L to the left and right. Horizontal bars and dots indicate domains and their centers for $L = 12$ (bottom) and $L = 24$ (top). Solid (dashed) vertical lines indicate domain interfaces (centers) for $L = 0$. Gray curves for $L = 0$ in (a) and (b) are the same as those in Fig. 5 (b) with same markers (green and blue, respectively).

versions of the PDFs using local regression [55]. The g_n^D show a degree of fluctuation increasing along n , which stems from the strong interference-induced p_n -fluctuations among individual configurations. They clearly demonstrate, though, an *enhancement in transfer efficiency when local symmetry is added* ($g_n^D > 1$), to chain parts dependent on the symmetry domains.

For $D = 1$ (global symmetry), the enhancement practically starts when crossing the symmetry center, and is then steadily increased in the right chain half. In similarity to the network case of Ref. [28], this is a consequence of the definite parity of the eigenstates under global reflection: When those parity eigenstates have a finite projection onto the initial input state (on the left chain half), they will enable tunneling to their mirror-related part (on the right half). The total transfer is determined by the combination of such effective “double-well” tunnelings [34]. For $D = 2$, the two local reflection operations $\mathcal{P}_{\mathbb{D}_{1,2}}$ do not commute with H , but still there is a multitude of *approximate* local parity eigenstates (see Sec. 2.2) which can assist in tunneling between the two halves of each domain. Indeed, we observe a drastically enhanced transfer to the right half ($n \in [36, 72]$) of \mathbb{D}_1 which stops roughly at the interface to \mathbb{D}_2 . Then g_n slightly drops, and increases again in the right half ($n \in [108, 144]$) of \mathbb{D}_2 . The scheme of increased enhancement in right domain halves is similar for $D = 3$. Note that the g_n -curves are scaled by the domain size: Their slopes are approximately the same in corresponding domain parts, with the slopes overall decreasing towards the right chain end.

The main difference to the global symmetry case is a generally significant portion of lr pair states as well as asymmetric domain-interface-localized states, depending on the fictitious intra-domain barriers (see Sec. 2.2). These states do not contribute to the intra-domain tunneling and therefore lower the transfer enhancement compared to the global symmetry case. For the weak disorder chosen in Fig. 5, the occurrence of such states is overall reduced, but at the same time *extended* asymmetric states are favored. Those may generally contribute to transfer, though also in the non-symmetric chain, and are therefore not expected to increase the g_n^D .

3.2. Overlap-induced transfer enhancement

Finally, an intriguing variation on the above LRD setups is to introduce spatial overlap between the domains \mathbb{D}_d (as in the explicit example of Fig. 4). We remark that such *domain overlap is a unique characteristic accessible with local symmetry* as opposed to global symmetry [38]. The key feature here is that symmetry-adapted LRD chain eigenstates (that is, eo and lr pairs as well as single approximate local parity eigenstates; see Sec. 2.2) of one domain may have substantial spatial overlap with those of a consecutive domain within the overlap region. Since an evolving wave-packet generally has contributions from all available eigenstates, it may be transferred across domains via this spatial overlap of different eigenstates.

Two such scenarios are realized in Fig. 6 for (a) $D = 2$ and (b) $D = 3$ symmetry domains, in two different ways (see horizontal bars indicating domains): In Fig. 6 (a) both domains are extended by L sites across the

middle of the chain (with equal domain sizes $N_1 = N_2 = N/2$ for $L = 0$), with their centers shifted by $L/2$, while in Fig. 6 (b) only the middle one of three equally sized domains is extended symmetrically by L , such that the domain centers remain fixed. In both cases, we observe a clear enhancement of transfer to the right half of the whole chain in the presence of domain overlap compared to adjacent domains ($L = 0$, gray curves).

Note that for $D = 2$, the overlap leads to a so-called *gapped translation symmetry* [42, 38]: The chain along the first $2L$ sites is repeated in (i. e., finitely “translated” to) the last $2L$ sites, but not in the region between which constitutes a symmetry “gap”; note though, that the mirror image of the translated part appears within the domain overlap. For $D = 3$, the overlap yields a *gapped reflection symmetry* [42, 38]: the chain is reflection-symmetric about its center, with the exception of the $N_d - 2L$ sites around the centers of \mathbb{D}_1 and \mathbb{D}_3 forming a (locally symmetric) gap. As it appears, those long-range correlations induced via overlap-induced gapped symmetries may play a substantial role in enhancing signal transfer through LRD systems. An interesting prospect would be to explore their impact for larger number of overlapping domains (of same or different sizes) featuring multiple symmetry gaps.

In the special case of $L = N/6$, for both ($D = 2, 3$) of the two considered LRD chain setups in Fig. 6 there is a dramatic enhancement of the ensemble-average transfer efficiency, with maximal g_n -factors reaching $g_n \approx 9$ (almost double the average maximal g_n for the globally symmetric setup in Fig. 5 (b)). Now, the $D = 2$ chain consists of a single part (first $2L$ sites) which is successively reflected two times at its right end, while the $D = 3$ chain becomes globally symmetric but additionally composed of two different symmetric units of size $2L$ (one in the middle and one repeated at the two ends). In particular, the latter case indicates that the possible transfer efficiency enhancement by global symmetry [28] may be even further *increased drastically if local symmetry is present simultaneously at smaller scales* within a composite system.

4. Conclusions

We have investigated the localization and signal transfer properties of finite, locally reflection-symmetric disordered (LRD) tight-binding chains, treating local symmetry as a spatial correlation of variable range. To reveal the localization behavior, we used the ensemble distributions of the inverse participation ratio (IPR) and a recently proposed measure of confinement here coined “cumulative Friedel sum” (CFS). It was shown that the spatial participation and fragmentation of eigenstates increases in the presence of local symmetries, and decreases towards the limit of uncorrelated disorder for increasing number of randomly sized symmetry domains, with statistical distributions depending on the disorder strength. The localization behavior is induced by the disordered symmetry domains acting as fictitious double wells in which eigenstates acquire approximate local parity. This type of symmetrized localization is explained within a local resonant scattering picture combined with the recent theory of effective confinement potentials. Further, the dynamics of a wave-packet upon excitation of the leftmost site in LRD chains was investigated in terms of the site-resolved transfer efficiency. Here, a systematic enhancement of transfer to the right halves of one, two, or three symmetry domains was shown to take place compared to the non-symmetric random chain. This enhancement can be drastically increased in the presence of overlap between symmetry domains; especially in the case of repeated extended constituents in the chain, or in the simultaneous presence of global and local reflection symmetry. In particular, the possibility to amplify signal transfer by the coexistence of global and local symmetry in composite systems is thus demonstrated.

We stress that the aim of the present work is to investigate the generic impact of the presence of local symmetry on localization and state transfer efficiency in a minimalistic setting. Disordered 1d chains with uniformly random potential were thus chosen as a platform to isolate the effect solely of the imposed symmetry—that is, without the influence of other structural characteristics or assumptions. We also underline that our results concern the properties of *finite* LRD chains, and are not to be seen as a study of correlations in approximants of the $N \rightarrow \infty$ limit; chain sizes were simply chosen large enough to perform statistics and vary the number or size of symmetry domains.

Certainly, many alternative routes could be employed to optimize the parameters of LRD setups for efficiency or to probe the effect of local symmetries with improved symmetry-adapted measures. The insight provided here may then also be leveraged to *design* devices with (overlapping) local symmetries, in order to achieve controllable localization or signal transfer at desired locations. As an example, we mention the perspective to combine the concept of overlapping local symmetries with the phenomenon of so-called “necklace

states” [5, 56] of spatially and spectrally overlapping resonances to achieve, e. g., simultaneous spatial confinement and transmission control. Alternatively, local symmetries may be applied to special types of structured disorder enabling engineered wave transport [57]. With the present work we take a step in the direction of understanding and manipulating the effect of coexisting local symmetries in a medium on its wave response, a concept which can be modeled in more complex systems and in higher dimensions.

5. Acknowledgements

P. S. acknowledges financial support by the Deutsche Forschungsgemeinschaft under grant DFG Schm 885/29-1. M. R. is thankful to the ‘Stiftung der deutschen Wirtschaft’ for financial support in the framework of a scholarship.

Appendix A. Local resonant scattering picture: localization and symmetrization from transparency

At the heart of the present study of LRD chains lies the tendency of eigenstates to localize into and symmetrize within symmetric domains, as described in Sec. 2.2—with asymmetric (but mirror-related) lr pair states resulting from combined quasidegenerate eo pair states perturbed by domain boundaries. We now give an intuitive argument for the symmetrized eigenstate localization in LRD chains, based on the combination of a recent unifying theory of wave localization [58] with a scattering picture of perfectly transmitting [43, 38] local resonant states. We split the argument by answering three questions, as follows.

Appendix A.1. Where in a disordered chain can an eigenstate localize?

To begin with, computing the eigenvectors of Eq. (3) for a generic disordered medium raises the question: What determines the positions and ranges of localization corresponding to given eigenvalues? The answer is provided in the fairly recently developed framework of “effective confining potentials” [59] and “localization landscapes” [58], formulated also for discrete models [52]. We now briefly outline this framework, and provide an example for an LRD chain in Fig. A.7 (a) (see below).

For our discrete chains, the so-called *effective confining potential* u_n is defined as the inverse of the “landscape function” τ_n , in turn given as the site amplitudes of the response $|\tau\rangle$ (solving $H_s |\tau\rangle = |e\rangle$) of the system to a spatially uniform excitation (source term) $|e\rangle$ [59, 52]:

$$u_n = \frac{1}{\tau_n} = \frac{1}{\langle n|\tau\rangle}, \quad |\tau\rangle = H_s^{-1} |e\rangle \quad (\text{A.1})$$

with $e_n = 1 \forall n$, where $H_s = H + V_s$ with a constant offset diagonal V_s added such that $u_n > 0$. As shown in Ref. [59], an eigenstate $|\phi^\nu\rangle$ of H with eigenenergy ϵ_ν decays exponentially within regions n where $\epsilon_\nu < u_n$, and can thus have substantial amplitude only in the remaining regions—that is, within local minima of u_n below the threshold ϵ_ν . In other words, u_n defines the locations to which ϕ_n^ν can be *spatially confined according to its energy*, namely between “effective barriers” where $\epsilon_\nu < u_n$. At larger ϵ_ν the eigenstate will be less localized, since such barriers between local u_n minima are exceeded and larger regions are available.

For discrete (tight-binding) models, eigenstates localize again for higher energies (like, e. g., state $|\phi^{489}\rangle$ in Fig. 2 (a)), though now confined by a so-called “dual” effective potential u'_n . It is obtained by using $H'_s = V'_s - H$ (with eigenenergies ϵ'_ν) instead of H_s in Eq. (A.1) where, again, the constant offset V'_s is added to have $u'_n > 0$. This is shown in Fig. A.7 (a) for a relatively high-energy eigenstate localizing into domain \mathbb{D}_5 of a LRD chain—here an example with $N = 10$ equally sized domains. The state is indeed confined between two thick effective barriers of the corresponding u'_n (where $\epsilon'_\nu < u'_n$) close to the borders of the domain. Smaller barriers lead to amplitude minima in the domain interior. Note here that u_n (and u'_n) follows the local symmetry of the original potential v_n .

Appendix A.2. Which possible location does an eigenstate choose to localize in?

Clearly, for a given level ϵ_ν , there are *multiple* local u_n (or u'_n) minima which could host the corresponding eigenstate; see e. g. the $\epsilon'_\nu < u'_n$ regions surrounding \mathbb{D}_5 in Fig. A.7 (a). As shown in Ref. [58] (and in a recent

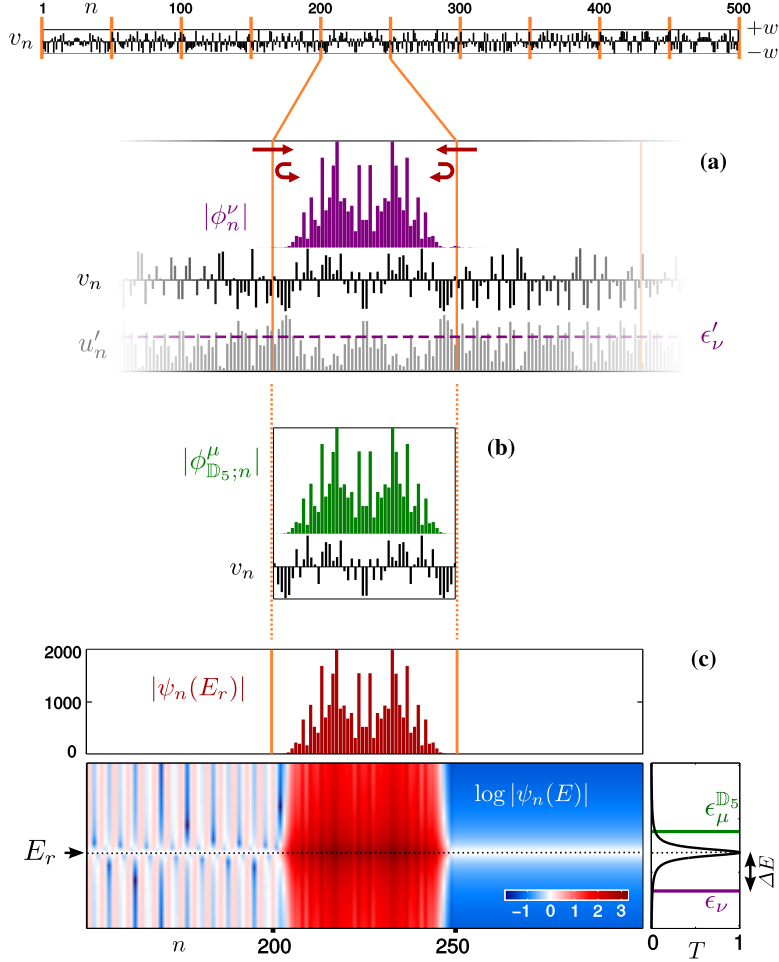


Figure A.7: **(a)**: Focus on eigenstate $\phi_n^{\nu=360}$ localized within domain \mathbb{D}_5 of an LRD chain (complete potential v_n in *top inset*, with domain interfaces indicated by vertical orange lines) with disorder strength $w = 3h$ and $D = 10$ domains of fixed size $N_d = N/D = 50$, together with dual effective confining potential u'_n (gray) and dual eigenenergy $\epsilon'_{\nu=360}$ (dashed horizontal line); see Eq. (A.1) and text below. **(b)**: Eigenstate $\phi_{\mathbb{D}_5;n}^{\mu=36}$ of isolated domain \mathbb{D}_5 (truncated chain potential shown in bottom). **(c)**: Perfectly transmitting ($T(E_r) = 1$) scattering state $\psi_n(E_r)$ (*top*) for plane wave incident on isolated domain \mathbb{D}_5 at resonant energy $E_r = \epsilon_{360} + \Delta E$ with $\Delta E \approx 3.6 \times 10^{-7} h$, and color-plot of scattering state map $\psi_n(E)$ on logarithmic scale (*bottom*) as well as transmission $T(E)$ (*bottom right*) in the vicinity of E_r , with eigenenergies $\epsilon_{\nu=360} = 1.265367 h$ (of $\phi_n^{\nu=360}$) and $\epsilon_{\mu=36}^{\mathbb{D}_5} \approx \epsilon_{360} + 1.55 \Delta E$ (of $\phi_{\mathbb{D}_5;n}^{\mu=36}$) indicated by horizontal lines. The transparency of \mathbb{D}_5 at E_r is indicated by straight arrows in (a), while round arrows indicate back-reflection from the neighboring domains, effectively leading to localization of ϕ_n^{ν} into \mathbb{D}_5 in a local scattering picture (see Appendix A.3). State moduli are plotted in arbitrary units in (a,b) and normalized to unit incoming flux in (c).

extension to discrete models [60]), the position where the eigenstate will actually localize is then determined by the minimal spectral distance

$$\delta\epsilon = \min_{\mathbb{C}, \mu} |\epsilon_{\nu} - \epsilon_{\mu}^{\mathbb{C}}| \quad (\text{A.2})$$

of the eigenenergy ϵ_{ν} to the eigenspectra $\{\epsilon_{\mu}^{\mathbb{C}}\}$ of sub-Hamiltonians $H_{\mathbb{C}}$ of (possible) domains of localization \mathbb{C} : The smaller $\delta\epsilon$ is for a given region \mathbb{C} , the larger is the allowed norm of $|\phi^{\nu}\rangle$ (eigenvector of H) within \mathbb{C} for given boundary data (in the present discrete case, values of ϕ_n^{ν} at the sites adjacent to \mathbb{C} [60]). Particularly, in the limiting case of zero boundary data, $\phi_n^{\nu} \neq 0$ only if $\epsilon_{\nu} = \epsilon_{\mu}^{\mathbb{C}}$ for some $H_{\mathbb{C}}$ -eigenstate $|\phi_{\mathbb{C}}^{\mu}\rangle$ under Dirichlet boundary conditions [58]. This essentially means that $|\phi^{\nu}\rangle$ will confine into the localization domain \mathbb{C} supporting a local $H_{\mathbb{C}}$ -eigenstate which best matches $|\phi^{\nu}\rangle$ in eigenenergy (i. e., with smallest $\delta\epsilon$). It will then also match it in spatial profile, that is, with (approximately) locally symmetric $|\phi_n^{\nu}|$ for symmetric $v_n \in \mathbb{C}$. An example of this is given in Fig. A.7 (b), showing the local eigenstate $|\phi_{\mathbb{C}}^{\mu=36}\rangle$ (where we have chosen $\mathbb{C} = \mathbb{D}_5$) matching $|\phi^{\nu=360}\rangle$ above of the full system which localizes in \mathbb{D}_5 .

As a side note, if the system contains repeated subdomains (not occurring in the present random potentials) such that corresponding repeated confining domains \mathbb{C} occur, then also the localization of an eigenstate will be repeated in those \mathbb{C} 's (since their $|\epsilon_{\nu} - \epsilon_{\mu}^{\mathbb{C}}|$ values will be equally small) with factors depending on the

detailed configuration at those domains' boundaries. This intuitively explains, e. g., the repeated amplitude patterns occurring in eigenstates of deterministic aperiodic structures [60] with correspondingly repeating sub-Hamiltonians, which feature abundant local symmetries at different scales [44].

Appendix A.3. Why is the chosen region of localization in the LRD chain symmetric?

Even within the above localization framework, however, the ultimate question of eigenstate symmetrization remains: Why does it happen that, for sufficiently strong localization, the domains \mathbb{C} with smallest $|\epsilon_\nu - \epsilon_\mu^{\mathbb{C}}|$, where the full eigenstates are confined, coincide with symmetry domains of the LRD chains?

To give an intuitive answer, let us view a subdomain \mathbb{D} as a local scatterer within a generic chain, and consider the scattering of a monochromatic wave of energy E incident from the left on the isolated \mathbb{D} connected to perfect semi-infinite chains (or “leads”). The transmission function $T(E) \in [0, 1]$, which is independent of the side of incidence of the wave, gives the portion of the (unit) wave amplitude that transmits through \mathbb{D} and leaves the scatterer on the right, while the reflected part is given by $R = 1 - T$. $T(E)$ naturally shows variations depending on the internal structure of \mathbb{D} and may, in particular, feature resonant peaks corresponding to quasibound states of the scatterer—with resonant widths proportional to the couplings of such states to the leads. Crucially, now, an energetically isolated resonance always has *perfect transmission* $T(E) = 1$ at the resonance position $E = E_r$ if the scatterer \mathbb{D} is symmetric, with resonant state spatial profile being symmetric [37, 43]. This is shown in Fig. A.7 (c) for scattering off the isolated domain \mathbb{D}_5 , which features a scattering resonance extremely close to the eigenenergy ϵ_{360} of the localized eigenstate in Fig. A.7 (a), with practically identical amplitude profile $|\psi_n(E_r)|$ (note the relative factor between $|\psi_{n \in \mathbb{D}_5}|$ within the scatterer and $|\psi_{n \notin \mathbb{D}_5}| = 1$ within the leads). This domain will thus be transparent at $E_r \approx \epsilon_{360}$ when embedded into the considered LRD chain, where eigenstates can be viewed as forming upon multiple scattering (and interference) of waves off local scatterers (as done also originally in, e. g., Anderson’s work [1]). In other words, waves impinging from the left and right onto \mathbb{D}_5 are let inside without reflection, while being reflected back into \mathbb{D}_5 by adjacent domains when reaching its border from inside, as indicated by arrows in Fig. A.7 (a). Thus, there will be an accumulation of amplitude in \mathbb{D}_5 forming the localized eigenstate at $\epsilon_{360} \approx E_r$, while this eigenstate is expelled from other localization regions due to larger $|\epsilon_{360} - \epsilon_\mu^{\mathbb{C}}|$, as discussed above.

The deviation from the above picture, that is, deviations of LRD chain eigenstate energies and profiles from local (perfectly transmitting) scattering resonance energies and profiles, increases with the leakage of the eigenstates through the symmetry domain boundaries. This naturally occurs for smaller disorder strength w relative to given eigenenergies, where disorder-induced spatial decay is weaker and, equivalently, more maxima in the effective confining potential u_n are exceeded by the eigenenergies.

Summarizing, eigenstate symmetrization into symmetry domains will occur for strong enough disorder (yielding short-range decay at the scale of the domain sizes), at eigenenergies matching perfect transmission resonance energies of the corresponding isolated domains. The link to the fictitious double wells defined in Appendix B can be viewed as follows. The effective confining potential of Eq. (A.1) governs the *details* of localization of an eigenstate. In the case of its symmetrization into a domain, its double-peak profile is represented by the simple picture of a fictitious double-well with corresponding strength and width.

Appendix B. Fictitious eigenstate-specific double wells

To provide a simple analysis tool relating the locally symmetrized eigenstates (see Appendix A) to the LRD chain characteristics, we here introduce an effective mapping of such eigenstates to corresponding local double wells.

Any finite piece of the disordered medium can be seen to act *effectively* as a homogeneous potential barrier, in the sense that both may lead to a spatially exponential decay of an eigenstate. In the uncorrelated disordered chain, an eigenstate $|\phi^\nu\rangle$ will typically be localized with an exponential decay of modulus envelope χ_n^ν , that is, $|\phi_n^\nu| \leq \chi_n^\nu \propto e^{-|n-n_\nu|/\ell}$, in both directions outwards from its maximum position denoted n_ν . Here, $\ell = \ell(\epsilon_\nu; w) \equiv 1/\gamma$ is the “localization length”, defined as the inverse of the so-called Lyapunov exponent γ , which generally depends on ϵ_ν and w [50]. On the other hand, for a homogeneous periodic chain with onsite potential $v_n = v$ and dispersion relation $E = 2h \cos k + v$ of H in Eq. (1), there are solutions exponentially decaying as $e^{-\kappa n}$ at imaginary momenta k (with $ik \equiv \kappa \in \mathbb{R}$) for energies E outside the band, $|E - v| > 2h$.

We thereby associate an exponentially localized state $|\phi^\nu\rangle$ in the uncorrelated disordered chain with a constant *fictitious potential barrier* of strength

$$\tilde{v}^\nu \equiv \epsilon_\nu - 2h \cosh \gamma(\epsilon_\nu; w), \quad (\text{B.1})$$

that is, supporting decaying states with the same exponent $\kappa = \gamma(\epsilon_\nu; w)$ at $E = \epsilon_\nu$.

Spatially, this fictitious barrier starts roughly at the sites adjacent to the single site, denoted n_ν , where $|\phi_n^\nu|$ is maximal. In the LRD chain, however, if an eigenstate is symmetrized in a domain \mathbb{D}_d , as described above, it has a second (local) maximum at the symmetry-related position $\mathcal{P}_{\mathbb{D}_d}(n_\nu)$; see e. g. $\phi^{\nu:\text{min}f}$ in Fig. 1. In this case, the fictitious barrier acquires a *finite width*, which we simply take to be the number of sites

$$\xi_d^\nu = |n_\nu - \mathcal{P}_{\mathbb{D}_d}(n_\nu)| - 1 = 2|n_\nu - c_d| - 1 \quad (\text{B.2})$$

between the positions of the two symmetry-related local maxima of state $|\phi^\nu\rangle$ localized in \mathbb{D}_d . This is visualized in the example of Fig. 2 (a), showing also \tilde{v} (superscripts dropped) for the selected state with an estimated $\ell = 1/\gamma = 0.8$ in Eq. (B.1). As a comparison, also the corresponding (fictitious) localized state denoted φ_n is shown, here produced by choosing a potential at n_ν and $\mathcal{P}_{\mathbb{D}_d}(n_\nu)$ (with \tilde{v} along the remaining chain) such that this state's energy matches ϵ_ν ⁵.

In the above situation, the interior of the symmetry domain \mathbb{D}_d effectively plays the role of a *symmetric double well* (like the globally symmetric setup of Ref. [34], but here coupled to adjacent sites), with a constant tunneling barrier of width ξ_d^ν and strength \tilde{v}^ν . The outer “walls” of this fictitious double well are represented by the constant potential \tilde{v}^ν on the left and right of n_ν and $\mathcal{P}_{\mathbb{D}_d}(n_\nu)$, respectively (see Fig. 2 (a)). Note that, even for a locally symmetrized state, the maximum position n_ν is still a stochastic variable, determined by the details of the random potential in (one half of) $\mathbb{D}_d \ni n_\nu$ for a given disorder configuration. In fact, the possible localization positions for given potential and eigenenergy can be found via the chain's “localization landscape”, as outlined in Appendix A. Distinct peaks at n_ν and $\mathcal{P}_{\mathbb{D}_d}(n_\nu)$ occur when $\xi_d^\nu \gg \ell(\epsilon_\nu; w)$, that is, when the fictitious tunneling barrier is sufficiently strong and/or wide. It may also often happen, however, that $\xi_d^\nu \sim \ell$, in which case the two fictitious wells practically merge into one, supporting a state peaked around the center c_d of \mathbb{D}_d .

Note that the localization length $\ell = \ell(\epsilon_\nu; w)$, indirectly determining each barrier strength via Eq. (B.1), generally depends in an involved manner on the energy and the disorder strength [50]. For the analysis carried out in the present work, it suffices to say that $\ell(\epsilon_\nu; w)$ overall decreases with increasing w and $|\epsilon_\nu|$ (for fixed w).

Appendix C. Eigenstate symmetrization statistics

The statistical distribution of the eigenstate IPR and CFS is analyzed in Sec. 2.3 in terms of the relative occurrence of locally even/odd or left-/right-localized states induced by local symmetry. To gain a more complete understanding of the localization and fragmentation for varying disorder strength w and number of symmetry domains D , we here provide a statistical analysis of the symmetrization properties of the same eigenstates used for the IPR and CFS statistics in Fig. 3.

To this end, we first label a given state $|\phi^\nu\rangle$ as “domain-localized” into a domain $\mathbb{D} \equiv \mathbb{D}^\nu$, if its total density $\sum_{n \in \mathbb{D}^\nu} \rho_n$ within this domain exceeds a threshold value which we set to 0.95. For each such domain-localized state we define the domain “density asymmetry”

$$\delta_\nu = \left| \sum_{n \in \mathbb{D}^\nu} [\rho_n - \rho_{\mathcal{P}_{\mathbb{D}^\nu}(n)}] \right| \quad (\text{C.1})$$

with respect to local reflection $\mathcal{P}_{\mathbb{D}^\nu}$ in this domain. For a given LRD chain, we then define N_{lr} as the number of eigenstates which have $\delta_\nu \geq \delta_{\text{thr}} \equiv 0.95$ (which are thus approximately confined to the left or right half

⁵Recall that, in contrast to a continuous potential, the barrier strength \tilde{v}^ν need not exceed the eigenenergy for the eigenstate to decay exponentially: The eigenenergy here merely needs to lie outside the allowed band of real Bloch momenta for a homogeneous chain with potential $v_n = \tilde{v}^\nu$, that is, to fulfill the condition $|E - v| > 2h$. In particular, \tilde{v}^ν may also well be negative (like in Fig. 2 (a)), and therefore we call it “strength” instead of “height”.

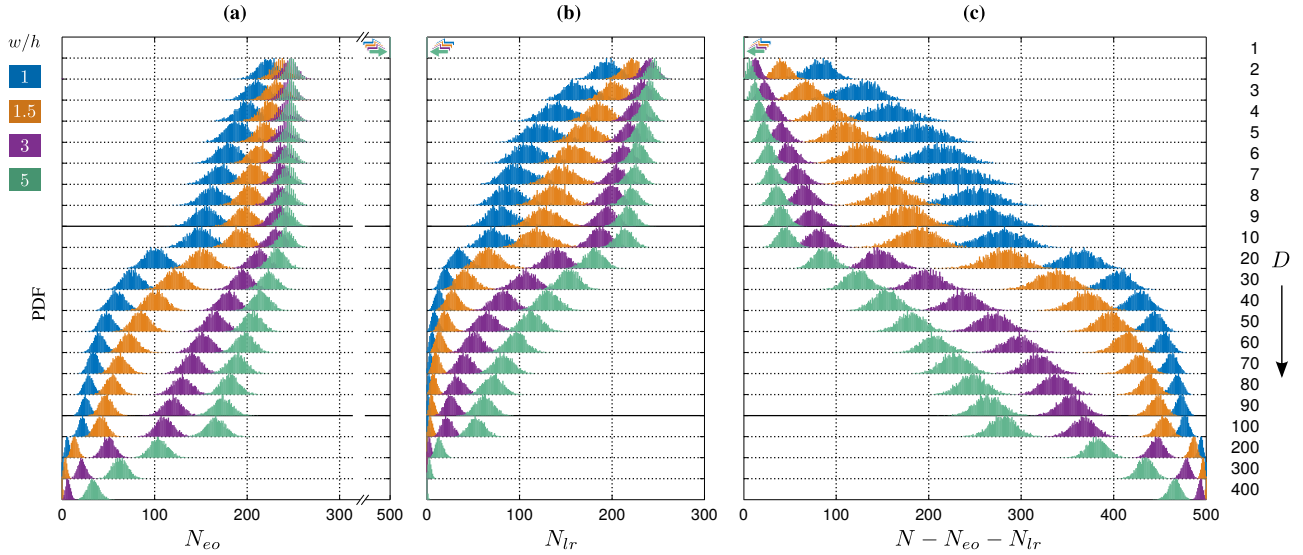


Figure C.8: PDFs of the number of approximate (a) locally even or odd eigenstates N_{eo} , (b) locally left- or right-localized eigenstates N_{lr} , and (c) remaining eigenstates $N - N_{eo} - N_{lr}$ (as defined in Appendix C) for varying w and D , using the same ensemble of LRD chains as in Fig. 3. The colored arrows for $D = 1$ indicate a single bar at (a) $N_{eo} = 500$, (b) $N_{lr} = 0$, and (c) $N - N_{eo} - N_{lr} = 0$, for all w -values. PDFs are normalized to maximum for each parameter combination.

of \mathbb{D}^ν), and as N_{eo} the number of eigenstates with $\delta_\nu < 1 - \delta_{\text{thr}}$ (which are approximately even or odd under $\mathcal{P}_{\mathbb{D}^\nu}$). The remaining $N - N_{eo} - N_{lr}$ eigenstates are those which either do not localize to 95% in a single symmetry domain, or do but do not reach 95% density symmetry or asymmetry.

Note that N_{eo} counts the even-odd *pair* states described in Sec. 2.2, but also single locally even or odd states with no quasidegenerate partner. Similarly, N_{lr} counts the left-right *pair* states, but also single left- or right-localized states with no quasidegenerate partner. Further, we point out that the above (global) threshold values are here simply chosen empirically to describe the present localization behavior; they could be relaxed to include less localized or non-symmetrized states in N_{eo} and N_{lr} , or in principle also be refined to depend, e. g., on w .

In Fig. C.8 the PDFs (histograms) of N_{eo} , N_{lr} , and the remainder $N - N_{eo} - N_{lr}$ are shown for the LRD chain ensembles used in Fig. 3, with varying disorder strength w and number of symmetry domains $D \geq 1$. For globally symmetric chains ($D = 1$) all states are even or odd, as evident from the single bars at $N_{eo} = N = 500$ and $N_{lr} = 0$ at any w . For locally symmetric chains ($D > 1$), N_{eo} and N_{lr} are in general larger at stronger disorder, since the states are then more short-range-localized and thus less prone to leakage through domain interfaces. For increasing D , we see that both N_{eo} and N_{lr} decrease at any w , since the domains become smaller on average, making interface localization as well as extension across domains more probable. We also notice, however, that N_{lr} decreases faster with D than N_{eo} . This predominance of locally even/odd states (which are overall more spatially fragmented) over left/right-localized states is in accordance with the CFS-distribution peaks at lower \bar{f} -values in Fig. 3.

Appendix D. IPR and CFS for random versus globally symmetric chains

The downward jump of the mean IPR and, much more drastically, mean CFS distributions in Fig. 3 when switching on global symmetry (from $D = 0$ to $D = 1$) is here detailed in terms of individual r_ν and f_ν eigenstate profiles before averaging, and further analyzed for larger chain sizes N .

Specifically, we consider in Fig. D.9 a random chain (left column, $D = 0$) and its symmetrized version (right column, $D = 1$), for which we present the complete distribution of r_ν and f_ν of all eigenstates $|\phi^\nu\rangle$, for the disorder strengths also used in Sec. 2.3 (top to bottom panels). Since the f_ν are relatively close to unity in the $D = 0$ case, we plot the difference $f_\nu - 1$ (further magnified by global factors for $D = 0$) to increase visibility. Additionally, for each (w, D) -combination we show those eigenstates ϕ^ν corresponding to the r_ν and f_ν closest to the mean values \bar{r} and \bar{f} (indicated by the small horizontal bars on the right of each panel),

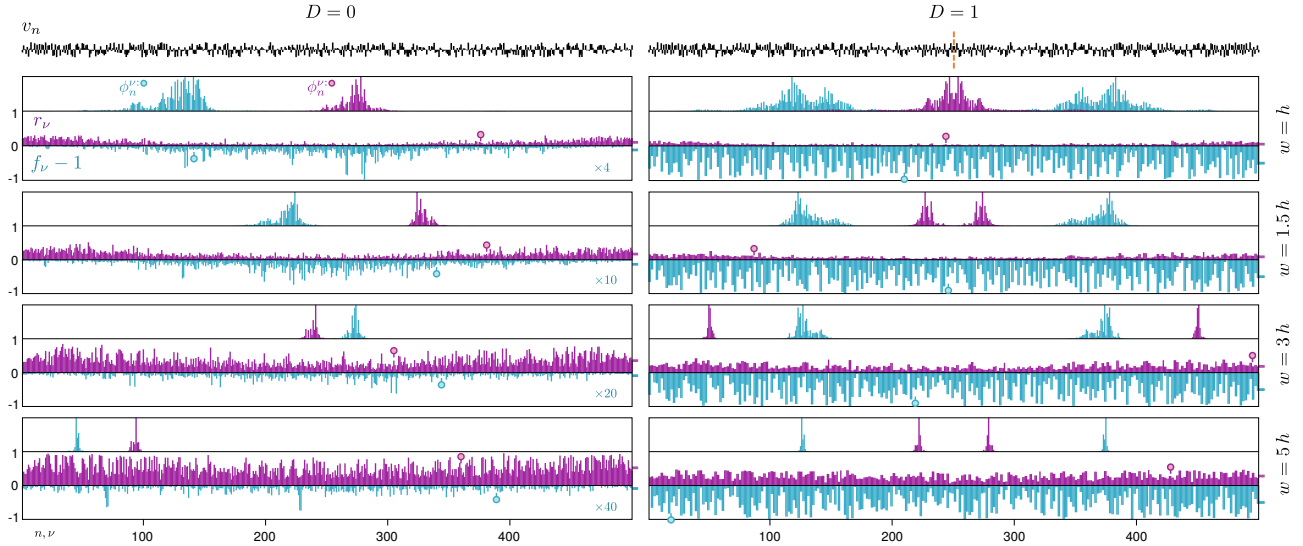


Figure D.9: IPRs r_ν and CFSs f_ν of eigenstates $|\phi^\nu\rangle$, sorted in eigenenergies ϵ_ν , of (left column) a random and (right column) a globally reflection-symmetric disordered chain of size $N = 500$, with (top to bottom) varying disorder strength w applied to the same potential configuration v_n shown in the top insets. The right setup ($D = 1$) is the left setup ($D = 0$) symmetrized; the dashed vertical line indicates the symmetry axis. The difference of f_ν from 1 is plotted (magnified in left column by the indicated factors) for better visibility. In each panel, the purple (blue) circle marks the state ϕ^ν shown in the top row, corresponding to the r_ν (f_ν) closest to the mean \bar{r} (\bar{f}) indicated by colored horizontal bars on the right. State magnitudes normalized to maximum are plotted.

respectively. They provide representatives of the kind of spatial profiles contributing to the statistical \bar{r} - and \bar{f} -distribution peaks.

As expected, for the random chain ($D = 0$) the states simply become more localized when increasing w (indicated also from the representative states shown), such that also the r_ν and f_ν overall increase (the f_ν get closer to 1). Further, states closer to the middle of the energy range for each setup are generally more extended, especially for weak disorder, as evident from the smaller r_ν - and f_ν -values there.

When turning on global symmetry ($D = 1$), all states have reflection-symmetric density, and especially the f_ν -distributions change drastically: They are shifted to much smaller values overall, with their mean \bar{f} close to $1/2$ for any w . Indeed, the shown representative states have density peaks symmetrically located about halfway from the center to the end of the chain (i.e., spacing $\xi \approx N/2$), yielding $f_\nu \approx 1/2$ (recall the description in Sec. 2.1). Also, the fluctuations of the f_ν around \bar{f} are rather homogeneous along the energy range, in contrast to the $D = 0$ cases; there is no suppression of the f_ν around the center, even for small w . This occurs because the CFS depends primarily on the spacing of the density peaks, which can vary similarly for different ϵ_ν as well as w , and rather less on the localization around the peaks themselves. These features are not captured by the IPR, which is merely sensitive to the total site participation of a given density profile: Since each state is globally symmetrized for $D = 1$, it contributes spatially by a double amount of sites, and the IPRs are approximately halved compared to the corresponding $D = 0$ setup (see also below).

The above behavior of the state-resolved r_ν and f_ν are in accordance with the peak values observed in the IPR and CFS distributions for $D = 0, 1$ in Fig. 3, which we now show remain similar for longer chains. Figure D.10 shows the PDF of the IPRs and CFSs for chains of length $N = 500, 1000, 2000$, with no symmetry and with global symmetry, for varying w . For the IPR, we see that the peak \bar{r} -values remain practically the same when changing N (since the spatial “participation” of the states does not change on average) and are halved when turning on the symmetry (whence the participation is doubled). For the CFS, we firstly observe that the peak \bar{f} -values jump to $1/2$ when imposing global symmetry, as explained above, for all chain lengths N . On the other hand, for $D = 0$ the PDFs are shifted to larger \bar{f} . This is because the CFS depends on the relative extent of a state to the total chain size: Its cumulative summand (see Eq. (5)) increases when the portion of sites with vanishing density increases. For all cases, we also see that the overall statistical fluctuations of the \bar{r} - and \bar{f} -distributions around their peak values decrease with increasing N .

Finally, a technical remark is in order. Computing the statistical IPR and CFS distributions (here for 3000

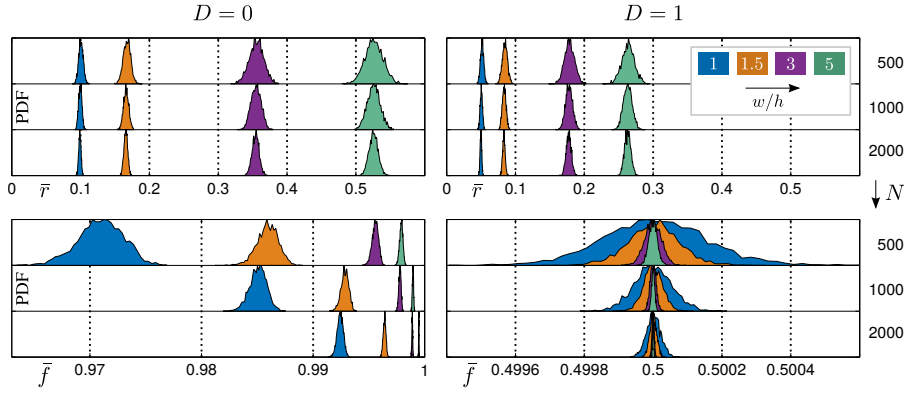


Figure D.10: PDFs of the mean (*top panels*) IPR \bar{r} and (*bottom panels*) CFS \bar{f} for chains with (*left panels*) no and (*right panels*) global reflection symmetry, for different chain lengths N and varying disorder strength w , using 3000 configurations for each parameter combination.

configurations) of the longer chains ($N = 1000, 2000$) would be prohibitive computationally at the precision necessary to guarantee the definite parity of all eigenstates in the $D = 1$ case [54]. Therefore, we have here exploited the global symmetry to bring the Hamiltonian H into a block-diagonal form with the same spectrum, with the parity-definite eigenvectors obtained from those of the blocks.

Specifically, for $D = 1$, H is a real centrosymmetric tridiagonal matrix which, following the procedure described in e. g. Ref. [61], can be block-decomposed into the two matrices

$$H^\pm = \begin{bmatrix} v_1 & h & & & & \\ h & v_2 & h & & & \\ & \ddots & \ddots & \ddots & & \\ & & h & v_{N/2-1} & h & \\ & & & h & v_{N/2} \pm h & \end{bmatrix} \quad (\text{D.1})$$

of halved size for even N . If $x^\mu = [x_1^\mu, \dots, x_{N/2}^\mu]^\top$ ($\mu = 1, \dots, N/2$) is an eigenvector of H^\pm with eigenvalue ϵ_\pm^μ , then

$$[x_1^\mu, \dots, x_{N/2}^\mu, \pm x_{N/2}^\mu, \dots, \pm x_1^\mu]^\top \quad (\text{D.2})$$

is an eigenvector of H with the same eigenvalue. Thus, all eigenvalues and associated (even or odd) eigenvectors of H are obtained, while the matrices H^\pm can be diagonalized using standard double precision arithmetic (with, e. g., the `eig` function in MATLAB[®]).

Note that a decomposition of H like above is not applicable to *locally* reflection-symmetric chains, where the corresponding local site permutations do not commute with H . Thus, computing eigenstates for $D > 1$ would require ever increasing arithmetic precision for increasing N , especially for large w . We stress, however, that the purpose of the present study is *not* to capture the effect of local symmetries in the large N limit, but the dependence on the number of symmetry domains D in *finite* chains. The size $N = 500$ of the LRD chains is simply chosen large enough (a) to be able to vary D of a substantial range and (b) to extract a meaningful statistics (e. g. the mean \bar{r} and \bar{f}) from individual chains. In fact, in the $N \rightarrow \infty$ limit any (finite) local symmetry domain would be of negligible relative size, and thus adjacent domains would simply behave as random consecutive scatterers, each with some internal structure and multiple resonant levels.

Appendix E. Eigenenergy spectra of LRD chains

In Fig. 1 of the main text, the scale of the energy axis is too small to discern the effect of the local symmetries of the chain on its spectrum, which we briefly comment on here.

In fact, the spectrum of an LRD chain closely resembles that of an uncorrelated random chain: For sufficiently strong disorder, the eigenstates are so spatially localized that their eigenenergies (with contributions from the onsite potentials where the state magnitude is non-vanishing) are also uncorrelated; there is no so-called ‘‘level repulsion’’ between states. Thus, the ϵ_ν follow a roughly linear trend in the bulk of the spectrum,

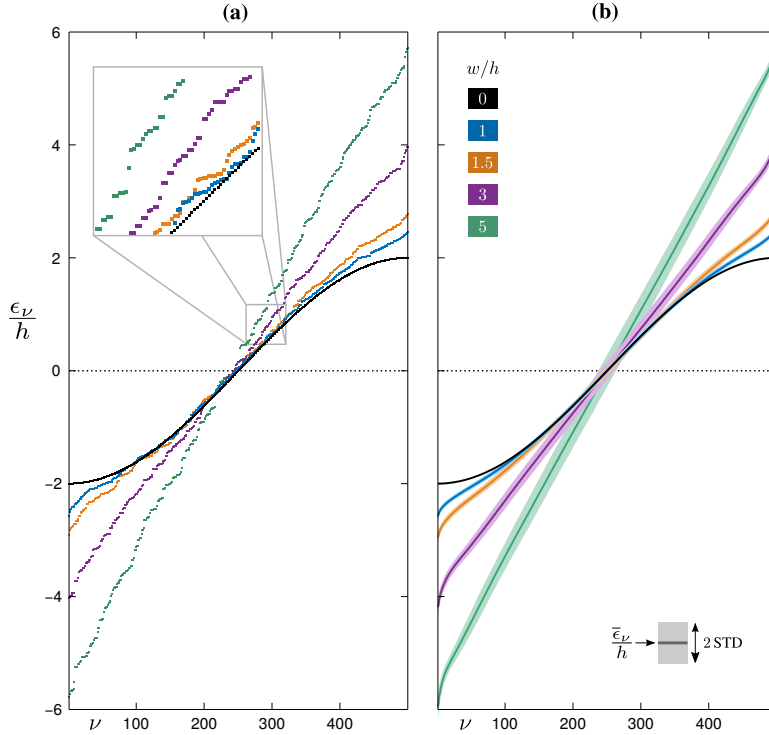


Figure E.11: **(a)** Eigenenergy spectra ϵ_ν of the LRD chain configuration of Fig. 1 (with $D = 10$ symmetry domains) for varying disorder strength w , and **(b)** ensemble average (solid lines) of 3000 LRD configurations with the same D, w as in (a), plotted on top of shaded stripes of width equal to two standard deviations at each ν . The inset in (a) reveals details of the single spectrum including multiple quasidegeneracies for larger w .

possibly with some additional low- or high-energy states at the ends of the spectrum (corresponding to states which happen to localize strongly on very low or high onsite potentials, respectively).

The only difference when imposing local reflection symmetries on a random chain is that multiple eo and lr state pairs may form, as explained in Sec. 2.2, leading to corresponding quasidegeneracies in the spectrum. Those can be distinguished in the inset of Fig. E.11 (a) showing the spectra of the LRD chain of Fig. 1 for different disorder strengths (the $w = 3h$ spectrum is that of Fig. 1). These quasidegeneracies do not affect the linear trend of ϵ_ν on larger scale for large w . They rather lead to a stronger fluctuation around the average spectrum $\bar{\epsilon}_\nu$ of the ensemble (of equivalent configurations) shown in Fig. E.11 (b). Indeed, the standard deviation is measured to be a global factor ≈ 1.38 larger than that for random chains without symmetries (not shown) for all considered w .

With decreasing w , the eigenstates become less localized, quasidegeneracies between eo -pair states and lr -pair states are gradually lifted (see inset in Fig. E.11 (a)). The spectra approach the unperturbed spectrum of a homogeneous chain (shown in black in Fig. E.11). This is manifest more clearly in the ensemble average in Fig. E.11 (b). There, we also see that the standard deviation around $\bar{\epsilon}_\nu$ naturally decreases towards the limit of the clean chain.

Finally, a comment is in order regarding the level spacing statistics of the considered model, as such a treatment is commonly used to characterize properties of disordered systems. It is clear from the above that the level statistics will overall follow that of a chain with uncorrelated disorder, though with an increased contribution to spacings very close to zero at sufficient disorder strength, due to the quasidegeneracies induced by the local reflection symmetries. Specifically, for relatively strong disorder the level spacings $\Delta\epsilon_\nu$ qualitatively follow a Poisson-like distribution with an additional enhancement for $\Delta\epsilon_\nu \rightarrow 0$. When the disorder strength is lowered, a transition to Wigner-Dyson-like level statistics occurs due to level repulsion [62]. Also the symmetry-induced quasidegeneracies are then increasingly lifted, since those levels repel each other too, thus depleting the contribution at $\Delta\epsilon_\nu \rightarrow 0$. For all disorder strength values w considered in the present context, however, the distributions remain practically Poisson-like, even for the weakest disorder with $w = h$. We therefore refrain from presenting a study of level spacings for the model, which would additionally require a significant variation of parameters as well as larger chain sizes to be conclusive. We emphasize, however,

that the purpose here is to analyze the impact of local reflection symmetries on the eigenstates and transfer behavior of an explicitly finite chain. A targeted statistical spectral analysis of the long chain limit is left as an interesting direction for future work.

References

- [1] P. W. Anderson, “Absence of Diffusion in Certain Random Lattices,” *Phys. Rev.* **109**, 1492 (1958).
- [2] D. J. Thouless, “Electrons in disordered systems and the theory of localization,” *Phys. Rep.* **13**, 93 (1974).
- [3] T. Schwartz, G. Bartal, S. Fishman, and M. Segev, “Transport and Anderson localization in disordered two-dimensional photonic lattices,” *Nature* **446**, 52 (2007).
- [4] M. Segev, Y. Silberberg, and D. N. Christodoulides, “Anderson localization of light,” *Nat. Phot.* **7**, 197 (2013).
- [5] J. Bertolotti, S. Gottardo, D. S. Wiersma, M. Ghulinyan, and L. Pavesi, “Optical Necklace States in Anderson Localized 1D Systems,” *Phys. Rev. Lett.* **94**, 113903 (2005).
- [6] H. H. Sheinfux, I. Kaminer, A. Z. Genack, and M. Segev, “Interplay between evanescence and disorder in deep subwavelength photonic structures,” *Nat. Commun.* **7**, 12927 (2016).
- [7] J. Billy, V. Josse, Z. Zuo, A. Bernard, B. Hambrecht, P. Lugan, D. Clément, L. Sanchez-Palencia, P. Bouyer, and A. Aspect, “Direct observation of Anderson localization of matter waves in a controlled disorder,” *Nature* **453**, 891 (2008).
- [8] G. Roati, C. D’Errico, L. Fallani, M. Fattori, C. Fort, M. Zaccanti, G. Modugno, M. Modugno, and M. Inguscio, “Anderson localization of a non-interacting Bose–Einstein condensate,” *Nature* **453**, 895 (2008).
- [9] M. Pasek, G. Orso, and D. Delande, “Anderson Localization of Ultracold Atoms: Where is the Mobility Edge?” *Phys. Rev. Lett.* **118**, 170403 (2017).
- [10] H. E. Kondakci, A. F. Abouraddy, and B. E. A. Saleh, “A photonic thermalization gap in disordered lattices,” *Nat. Phys.* **11**, 930 (2015).
- [11] H. E. Kondakci, A. Szameit, A. F. Abouraddy, D. N. Christodoulides, and B. E. A. Saleh, “Sub-thermal to super-thermal light statistics from a disordered lattice via deterministic control of excitation symmetry,” *Optica* **3**, 477 (2016).
- [12] U. Naether, S. Stützer, R. A. Vicencio, M. I. Molina, A. Tünnermann, S. Nolte, T. Kottos, D. N. Christodoulides, and A Szameit, “Experimental observation of superdiffusive transport in random dimer lattices,” *New J. Phys.* **15**, 013045 (2013).
- [13] U. Naether, J. M. Meyer, S. Stützer, A. Tünnermann, S. Nolte, M. I. Molina, and A. Szameit, “Anderson localization in a periodic photonic lattice with a disordered boundary,” *Opt. Lett.* **37**, 485 (2012).
- [14] F. M. Izrailev, A. A. Krokhin, and N. M. Makarov, “Anomalous localization in low-dimensional systems with correlated disorder,” *Phys. Rep.* **512**, 125 (2012).
- [15] M. Titov and H. Schomerus, “Nonuniversality of Anderson Localization in Short-Range Correlated Disorder,” *Phys. Rev. Lett.* **95**, 126602 (2005).
- [16] M. O. Sales and F. A. B. F. de Moura, “Numerical study of the one-electron dynamics in one-dimensional systems with short-range correlated disorder,” *Physica E* **45**, 97 (2012).
- [17] D. H. Dunlap, H.-L. Wu, and P. W. Phillips, “Absence of localization in a random-dimer model,” *Phys. Rev. Lett.* **65**, 88 (1990).

- [18] F. C. Lavarda, M. C. dos Santos, D. S. Galvão, and B. Laks, “Near Resonant Scattering from Nonsymmetric Dimers: Applications to Substituted Polyanielines,” *Phys. Rev. Lett.* **73**, 1267 (1994).
- [19] A. Sánchez, E. Maciá, and F. Domínguez-Adame, “Suppression of localization in Kronig-Penney models with correlated disorder,” *Phys. Rev. B* **49**, 147 (1994).
- [20] P. K. Datta and K. Kundu, “The absence of localization in one-dimensional disordered harmonic chains,” *J. Phys.: Condens. Mat.* **6**, 4465 (1994).
- [21] F. M. Izrailev and A. A. Krokhnin, “Localization and the Mobility Edge in One-Dimensional Potentials with Correlated Disorder,” *Phys. Rev. Lett.* **82**, 4062 (1999).
- [22] D. López-González and M. I. Molina, “Transport of localized and extended excitations in chains embedded with randomly distributed linear and nonlinear n -mers,” *Phys. Rev. E* **93**, 032205 (2016).
- [23] F. A. B. F. de Moura and M. L. Lyra, “Delocalization in the 1D Anderson Model with Long-Range Correlated Disorder,” *Phys. Rev. Lett.* **81**, 3735 (1998).
- [24] H. Cheraghchi, S. M. Fazeli, and K. Esfarjani, “Localization-delocalization transition in a one-dimensional system with long-range correlated off-diagonal disorder,” *Phys. Rev. B* **72**, 174207 (2005).
- [25] A.-M. Guo and S.-J. Xiong, “Suppression of localization in a two-leg ladder model with correlated binary disorder,” *Phys. Rev. B* **83**, 245108 (2011).
- [26] F. A. B. F. de Moura, F. F. S. Leão, and M. L. Lyra, “Resonant states and wavepacket super-diffusion in intra-chain correlated ladders with diluted disorder,” *J. Phys.: Condens. Mat.* **23**, 135303 (2011).
- [27] R. C. P. Carvalho, M. L. Lyra, F. A. B. F. de Moura, and F. Domínguez-Adame, “Localization on a two-channel model with cross-correlated disorder,” *J. Phys.: Condens. Mat.* **23**, 175304 (2011).
- [28] T. Zech, R. Mulet, T. Wellens, and A. Buchleitner, “Centrosymmetry enhances quantum transport in disordered molecular networks,” *New J. Phys.* **16**, 055002 (2014).
- [29] M. Walschaers, J. F.-d.-C. Diaz, R. Mulet, and A. Buchleitner, “Optimally Designed Quantum Transport across Disordered Networks,” *Phys. Rev. Lett.* **111**, 180601 (2013).
- [30] M. Walschaers, R. Mulet, T. Wellens, and A. Buchleitner, “Statistical theory of designed quantum transport across disordered networks,” *Phys. Rev. E* **91**, 042137 (2015).
- [31] M. Walschaers, F. Schlawin, T. Wellens, and A. Buchleitner, “Quantum Transport on Disordered and Noisy Networks: An Interplay of Structural Complexity and Uncertainty,” *Annu. Rev. Condens. Matter Phys.* **7**, 223 (2016).
- [32] A. Ortega, T. Stegmann, and L. Benet, “Efficient quantum transport in disordered interacting many-body networks,” *Phys. Rev. E* **94**, 042102 (2016).
- [33] A. Ortega, T. Stegmann, and L. Benet, “Robustness of optimal transport in disordered interacting many-body networks,” *Phys. Rev. E* **98**, 012141 (2018).
- [34] E. Diez, F. Izrailev, A. Krokhnin, and A. Rodriguez, “Symmetry-induced tunneling in one-dimensional disordered potentials,” *Phys. Rev. B* **78**, 035118 (2008).
- [35] H. Zabrodsky, S. Peleg, and D. Avnir, “Continuous symmetry measures,” *J. Am. Chem. Soc.* **114**, 7843 (1992).
- [36] M. Pinsky, D. Casanova, P. Alemany, S. Alvarez, D. Avnir, C. Dryzun, Z. Kizner, and A. Sterkin, “Symmetry operation measures,” *J. Comput. Chem.* **29**, 190 (2008).
- [37] P. A. Kalozoumis, C. Morfonios, F. K. Diakonov, and P. Schmelcher, “Local symmetries in one-dimensional quantum scattering,” *Phys. Rev. A* **87**, 032113 (2013).

- [38] C. V. Morfonios, P. A. Kalozoumis, F. K. Diakonou, and P. Schmelcher, “Nonlocal discrete continuity and invariant currents in locally symmetric effective Schrödinger arrays,” *Ann. Phys.* **385**, 623 (2017).
- [39] M. Röntgen, C. V. Morfonios, F. K. Diakonou, and P. Schmelcher, “Non-local currents and the structure of eigenstates in planar discrete systems with local symmetries,” *Ann. Phys.* **380**, 135 (2017).
- [40] P. A. Kalozoumis, C. V. Morfonios, F. K. Diakonou, and P. Schmelcher, “ \mathcal{PT} -symmetry breaking in waveguides with competing loss-gain pairs,” *Phys. Rev. A* **93**, 063831 (2016).
- [41] T. Wulf, C. V. Morfonios, F. K. Diakonou, and P. Schmelcher, “Exposing local symmetries in distorted driven lattices via time-averaged invariants,” *Phys. Rev. E* **93**, 052215 (2016).
- [42] P. A. Kalozoumis, C. Morfonios, F. K. Diakonou, and P. Schmelcher, “Invariants of Broken Discrete Symmetries,” *Phys. Rev. Lett.* **113**, 050403 (2014).
- [43] P. A. Kalozoumis, C. Morfonios, N. Palaiodimopoulos, F. K. Diakonou, and P. Schmelcher, “Local symmetries and perfect transmission in aperiodic photonic multilayers,” *Phys. Rev. A* **88**, 033857 (2013).
- [44] C. Morfonios, P. Schmelcher, P. A. Kalozoumis, and F. K. Diakonou, “Local symmetry dynamics in one-dimensional aperiodic lattices: A numerical study,” *Nonlin. Dyn.* **78**, 71 (2014).
- [45] J.-P. Allouche, M. Baake, J. Cassaigne, and D. Damanik, “Palindrome complexity,” *Theor. Comp. Sci.* **292**, 9 (2003).
- [46] P. Wochner, C. Gutt, T. Autenrieth, T. Demmer, V. Bugaev, A. D. Ortiz, A. Duri, F. Zontone, G. Grübel, and H. Dosch, “X-ray cross correlation analysis uncovers hidden local symmetries in disordered matter,” *P. Natl. Acad. Sci.* **106**, 11511 (2009).
- [47] M. Altarelli, R. P. Kurta, and I. A. Vartanyants, “X-ray cross-correlation analysis and local symmetries of disordered systems: General theory,” *Phys. Rev. B* **82**, 104207 (2010).
- [48] G. Couplier, C. Guthmann, Y. Noat, and M. S. Jean, “Local symmetries and order-disorder transitions in small macroscopic Wigner islands,” *Phys. Rev. E* **71**, 046105 (2005).
- [49] J. Echeverría, A. Carreras, D. Casanova, P. Alemany, and S. Alvarez, “Concurrent Symmetries: The Interplay Between Local and Global Molecular Symmetries,” *Chem. Eur. J.* **17**, 359 (2011).
- [50] A. Rodríguez, “One-dimensional models of disordered quantum wires: General formalism,” *J. Phys. A: Math. Gen.* **39**, 14303 (2006).
- [51] L. Gong, W. Li, S. Zhao, and W. Cheng, “A measure of localization properties of one-dimensional single electron lattice systems,” *Phys. Lett. A* **380**, 59 (2016).
- [52] M. L. Lyra, S. Mayboroda, and M. Filoche, “Dual landscapes in Anderson localization on discrete lattices,” *Europhys. Lett.* **109**, 47001 (2015).
- [53] D. C. Langreth, “Friedel Sum Rule for Anderson’s Model of Localized Impurity States,” *Phys. Rev.* **150**, 516 (1966).
- [54] All computations except those in [Appendix D](#) have been performed using the GMP (GNU Multiple Precision) arithmetic library implementation of LAPACK’s eigensolver in “MPACK”, a multiprecision linear algebra package developed by M. Nakata, available at <https://github.com/nakatamah/mpack>. Its “default precision” parameter was set to 768, 1024, 1280 for $w/h \leq 1, 3, 5$, respectively. Those were checked to be more than large enough to ensure that all eigenvectors of all globally symmetric setups ($D = 1$) are even or odd.
- [55] G. Marsh, “[LOESS regression smoothing](#),” MATLAB Central File Exchange (2016), retrieved January 2018; using `span` parameter (fraction of data used for fitting) = 0.1 (2018).

- [56] F. Sgrignuoli, G. Mazzamuto, N. Caselli, F. Intonti, F. S. Cataliotti, M. Gurioli, and C. Toninelli, “Necklace State Hallmark in Disordered 2D Photonic Systems,” [ACS Photonics](#) **2**, 1636 (2015).
- [57] A. Rodriguez, A. Chakrabarti, and R. A. Römer, “Controlled engineering of extended states in disordered systems,” [Phys. Rev. B](#) **86**, 085119 (2012).
- [58] M. Filoche and S. Mayboroda, “Universal mechanism for Anderson and weak localization,” [P. Natl. Acad. Sci.](#) **109**, 14761 (2012).
- [59] D. N. Arnold, G. David, D. Jerison, S. Mayboroda, and M. Filoche, “Effective Confining Potential of Quantum States in Disordered Media,” [Phys. Rev. Lett.](#) **116**, 056602 (2016).
- [60] M. Röntgen, C. V. Morfonios, R. Wang, L. D. Negro, and P. Schmelcher, “Local symmetry theory of resonator structures for the real-space control of edge-states in binary aperiodic chains,” [ArXiv180706812 Cond-Mat](#) (2018), [arXiv:1807.06812 \[cond-mat\]](#) .
- [61] M. Röntgen, C. V. Morfonios, and P. Schmelcher, “Compact localized states and flat bands from local symmetry partitioning,” [Phys. Rev. B](#) **97**, 035161 (2018).
- [62] F. Haake, *Quantum Signatures of Chaos*, [Springer-Verlag, Heidelberg](#) (2010).